View metadata, citation and similar papers at core.ac.uk

brought to you by CORE

provided by Elsevier - Publisher Connector

Available online at www.sciencedirect.com

SCIENCE DIRECT®

ELSEVIER

Journal of Computational and Applied Mathematics 197 (2006) 465–494

JOURNAL OF COMPUTATIONAL AND APPLIED MATHEMATICS

www.elsevier.com/locate/cam

Lie-group method for unsteady flows in a semi-infinite expanding or contracting pipe with injection or suction through a porous wall

Youssef Z. Boutros[a], Mina B. Abd-el-Malek[a,*,1], Nagwa A. Badran[a], Hossam S. Hassan[b]

[a] *Department of Engineering Mathematics and Physics, Faculty of Engineering, Alexandria University, Alexandria 21544, Egypt*
[b] *Department of Basic and Applied Science, Arab Academy for Science and Technology and Maritime Transport, P.O. Box 1029, Alexandria, Egypt*

Received 5 July 2005; received in revised form 14 November 2005

Abstract

The unsteady incompressible laminar flow in a semi-infinite porous circular pipe with injection or suction through the pipe wall whose radius varies with time is considered. The present analysis simulates the flow field by the burning of inner surface of cylindrical grain in a solid rocket motor, in which the burning surface regresses with time. We apply Lie-group method for determining symmetry reductions of partial differential equations. Lie-group method starts out with a general infinitesimal group of transformations under which given partial differential equations are invariant, then, the determining equations are derived [Ibragimov, Elementary Lie Group Analysis and Ordinary Differential Equations, Wiley, New York, 1999; Hydon, Symmetry Methods for Differential Equations, Cambridge University Press, Cambridge, 2000; Olver, Applications of Lie Groups to Differential Equations, Springer, New York, 1986; Seshadri, Na, Group invariance in engineering boundary value problems, Springer, New York, 1985; Yi, Fengxiang, Lie symmetries of mechanical systems with unilateral holonomic constraints, Chinese Sci. Bull. 45 (2000) 1354–1358; Moritz, Schwalm, Uherka, Finding Lie groups that reduce the order of discrete dynamical systems, J. Phys. A: Math. 31 (1998) 7379–7402; Nucci, Clarkson, The nonclassical method is more general than the direct method for symmetry reductions. An example of the Fitzhugh–Nagumo equation, Phys. Lett. A 164 (1992) 49–56; Basarab, Lahno, Group classification of nonlinear partial differential equations: a new approach to resolving the problem, Proceedings of Institute of Mathematics of NAS of Ukraine, vol. 43, 2002, pp. 86–92; Burde, Expanded Lie group transformations and similarity reductions of differential equations, Proceedings of Institute of Mathematics of NAS of Ukraine, vol. 43, 2002, pp. 93–101; Gandarias, Bruzon, Classical and nonclassical symmetries of a generalized Boussinesq equation, J. Nonlinear Math. Phys. 5 (1998) 8–12; Hill, Solution of Differential Equations by Means of One-Parameter Groups, Pitman Publishing Co., 1982]. The determining equations are a set of linear differential equations, the solution of which gives the transformation function or the infinitesimals of the dependent and independent variables. After the group has been determined, a solution to the given partial differential equation may be found from the invariant surface condition such that its solution leads to similarity variables that reduce the number of independent variables in the system. Effect of the cross-flow Reynolds number Re and the dimensionless wall expansion ratio α on velocity, flow streamlines, axial and radial pressure drop, and wall shear stress has been studied both analytically and numerically and the results are plotted.
© 2006 Elsevier B.V. All rights reserved.

MSC: 37L20; 35B20; 35Q30

Keywords: Navier–Stokes equations; Similarity solutions; Lie group; Small perturbations

* Corresponding author. Tel.: +20 3 391 8715; fax: +20 2 795 7565.
E-mail addresses: minab@aucegypt.edu (M.B. Abd-el-Malek), hossams@aast.edu (H.S. Hassan).
[1] Present address: Department of Mathematics, The American University in Cairo, Cairo 11511, Egypt.

0377-0427/$ - see front matter © 2006 Elsevier B.V. All rights reserved.
doi:10.1016/j.cam.2005.11.031

Nomenclature

A	injection coefficient
a	instantaneous wall radius, m
$\dot{a}$	wall expansion rate, m/s
$\bar{P}$	dimensional pressure, Pa
$\bar{r}$	radius, m
Re	cross-flow Reynolds number
t	time, s
$\bar{U}$	velocity $(\bar{u}, \bar{v})$, m/s
$\bar{u}$	axial velocity, m/s
$\bar{z}$	axial coordinate, m
ν	kinematic viscosity, m^2/s
$\bar{v}$	radial velocity, m/s
ρ	density, kg/m^3
Ψ	dimensionless stream function
ω	dimensionless vorticity
τ	dimensionless shear stress
α	dimensionless wall expansion ratio
μ	viscosity, kg/m s

1. Introduction

Goto and Uchida [4] analyzed the flow within a circular pipe when an incompressible fluid flows in through the wall surface while the radius of a semi-infinite circular pipe expands with time. They studied the case of expanding pipe with injection through wall. An exact similar solution is obtained through numerical calculation. The flow field is classified by the expansion ratio α, showing the expansion velocity of the pipe radius and the injection coefficient A, showing the injection velocity at the wall surface position.

The velocity distribution, pressure distribution and wall surface shearing stress are determined with the expansion ratio and injection coefficient as parameters through numerical calculation to clarify the influence of α and A on the flow field.

Magdalani et al. [8] studied higher mean-flow approximation for solid rocket motors with radially regressing walls. Rotational, incompressible, and viscous flow model that incorporates the effect of wall regression was used to describe the bulk gas motion in a circular-port rocket motor. They follow Goto and Uchida's approach [4] and write the stream function in a form that is consistent with mass conservation, namely, a Proudman–Johnson form [12]. The procedure involves a spatial transformation that presumes a linear varying axial velocity and a temporal transformation that is granted by a time-invariant dimensionless regression. When these transformations are applied to both space and time, the Navier–Stokes equations are reduced to a single, nonlinear, fourth-order differential equation. The resulting problem is solved using variation of parameters and small-parameter perturbations. The effect of injection Reynolds number Re and the dimensionless regression ratio α on the asymptotic solutions for the velocity, axial and normal pressure, vorticity, and shear stresses are obtained.

This paper is concerned with the solution of the Navier–Stokes equations which described the unsteady incompressible laminar flow in a semi-infinite porous circular pipe with injection or suction through the pipe wall whose radius varies with time. Lie-group method is applied to the equations of motion for determining symmetry reductions of partial differential equations. The resulting fourth-order nonlinear differential equation is then solved using small-parameter perturbations [14,15], and the results are compared with numerical solutions using shooting method coupled with Runge–Kutta scheme.

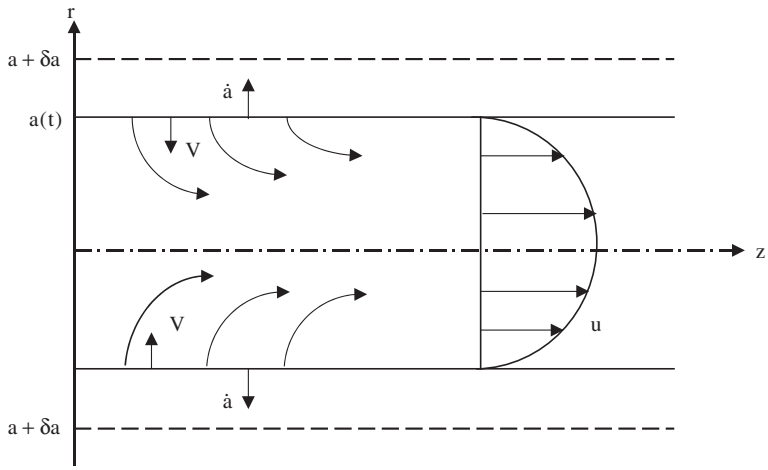

Fig. 1. Flow pattern in an expanding pipe.

2. Mathematical formulation of the problem

A circular pipe of a semi-infinite length with one end closed is considered. It is assumed that the pipe wall is porous and its radius varies with time. A coordinate system can be chosen based on axisymmetry as shown in Fig. 1.

The wall of the pipe moves only in the radial direction and expands at a speed equal to $\dot{a}$. The fluid is injected or sucked uniformly through the moving wall surface at velocity $v_w(=-V)$ at right angle to the wall surface and that is proportional to the moving velocity at the wall surface. In our analysis, we shall take the azimuthal component of the velocity to be zero and the kinematic viscosity is assumed to be constant.

The equations of continuity and of motion for an axisymmetric unsteady flow of incompressible fluid with no body forces, are given as follows:

$$\frac{\partial(\bar{r}\bar{u})}{\partial\bar{z}} + \frac{\partial(\bar{r}\bar{v})}{\partial\bar{r}} = 0, \tag{2.1}$$

$$\frac{\partial\bar{u}}{\partial t} + \bar{u}\frac{\partial\bar{u}}{\partial\bar{z}} + \bar{v}\frac{\partial\bar{u}}{\partial\bar{r}} = -\frac{1}{\rho}\frac{\partial\bar{P}}{\partial\bar{z}} + \nu\left[\frac{\partial^2\bar{u}}{\partial\bar{z}^2} + \frac{1}{\bar{r}}\frac{\partial}{\partial\bar{r}}\left(\bar{r}\frac{\partial\bar{u}}{\partial\bar{r}}\right)\right], \tag{2.2}$$

$$\frac{\partial\bar{v}}{\partial t} + \bar{u}\frac{\partial\bar{v}}{\partial\bar{z}} + \bar{v}\frac{\partial\bar{v}}{\partial\bar{r}} = -\frac{1}{\rho}\frac{\partial\bar{P}}{\partial\bar{r}} + \nu\left[\frac{\partial^2\bar{v}}{\partial\bar{z}^2} + \frac{\partial}{\partial\bar{r}}\left(\frac{1}{\bar{r}}\frac{\partial(\bar{r}\bar{v})}{\partial\bar{r}}\right)\right], \tag{2.3}$$

where the variables are given in the Nomenclature.

For time-dependent radius $\bar{r} = a(t)$, the boundary conditions will be

$$\begin{aligned}
&\text{(i) } \bar{u} = 0, \quad \bar{v} = \bar{v}_w = -V = -A\dot{a} \quad \text{at } \bar{r} = a(t),\\
&\text{(ii) } \frac{\partial\bar{u}}{\partial\bar{r}} = 0, \quad \bar{v} = 0 \quad \text{at } \bar{r} = 0,\\
&\text{(iii) } \bar{u} = 0 \quad \text{at } \bar{z} = 0.
\end{aligned} \tag{2.4}$$

In our analysis, we shall express the axial velocity, radial velocity and boundary conditions in terms of the stream function $\bar{\Psi}$. We can eliminate the pressure from the equations of motion (2.2) and (2.3) by using $\bar{P}_{\bar{z}\bar{r}}$ from (2.3) after differentiating it with respect to $\bar{z}$ into (2.2) after differentiating it with respect to $\bar{r}$. Finally we can get both axial and radial pressure drops in terms of the stream function.

From the continuity equation (2.1), there exists a dimensional stream function $\bar{\Psi}(\bar{z}, \bar{r}, t)$ such that

$$\bar{u} = \frac{1}{\bar{r}} \frac{\partial \bar{\Psi}}{\partial \bar{r}}, \quad \bar{v} = -\frac{1}{\bar{r}} \frac{\partial \bar{\Psi}}{\partial \bar{z}}, \tag{2.5}$$

which satisfies Eq. (2.1) identically.

If we introduce the dimensionless radial position $r = \bar{r}/a(t)$, Eq. (2.5) becomes

$$\bar{u} = \frac{1}{a^2 r} \frac{\partial \bar{\Psi}}{\partial r}, \quad \bar{v} = -\frac{1}{ar} \frac{\partial \bar{\Psi}}{\partial \bar{z}}. \tag{2.6}$$

Substituting (2.6) into (2.2) and (2.3) will lead to

$$\begin{aligned} &a^2 r^2 \bar{\Psi}_{rt} - a\dot{a} r^3 \bar{\Psi}_{rr} - a\dot{a} r^2 \bar{\Psi}_r + r \bar{\Psi}_r \bar{\Psi}_{r\bar{z}} - r \bar{\Psi}_{rr} \bar{\Psi}_{\bar{z}} + \bar{\Psi}_{\bar{z}} \bar{\Psi}_r \\ &\quad = -\frac{a^4 r^3}{\rho} \bar{P}_{\bar{z}} + \nu[a^2 r^2 \bar{\Psi}_{r\bar{z}\bar{z}} + r^2 \bar{\Psi}_{rrr} - r \bar{\Psi}_{rr} + \bar{\Psi}_r] \end{aligned} \tag{2.7}$$

and

$$-a^2 r^2 \bar{\Psi}_{\bar{z}t} + a\dot{a} r^3 \bar{\Psi}_{\bar{z}r} - r \bar{\Psi}_r \bar{\Psi}_{\bar{z}\bar{z}} + r \bar{\Psi}_{\bar{z}} \bar{\Psi}_{\bar{z}r} - (\bar{\Psi}_{\bar{z}})^2 = -\frac{a^3 r^3}{\rho} \bar{P}_r + \nu[-a^2 r^2 \bar{\Psi}_{\bar{z}\bar{z}\bar{z}} - r^2 \bar{\Psi}_{\bar{z}rr} + r \bar{\Psi}_{\bar{z}r}], \tag{2.8}$$

where subscripts denote partial derivatives.

The variables in Eqs. (2.7) and (2.8) are dimensionless according to

$$u = \frac{\bar{u}}{V}, \quad v = \frac{\bar{v}}{V}, \quad z = \frac{\bar{z}}{a(t)}, \quad \bar{t} = \frac{tV}{a}, \quad \Psi = \frac{\bar{\Psi}}{a^2 V}, \quad P = \frac{\bar{P}}{\rho V^2}, \quad \alpha = \frac{a\dot{a}}{\nu}. \tag{2.9}$$

Substituting (2.9) into (2.7) and (2.8) gives

$$\begin{aligned} &r^2 \Psi_{r\bar{t}} + r \Psi_r \Psi_{rz} + \Psi_z[\Psi_r - r \Psi_{rr}] + r^3 P_z \\ &\quad + \frac{1}{Re}[(r - \alpha r^3) \Psi_{rr} - r^2 \Psi_{rrr} - r^2 \Psi_{rzz} - (1 + \alpha r^2) \Psi_r] = 0 \end{aligned} \tag{2.10}$$

and

$$r^2 \Psi_{z\bar{t}} + r \Psi_r \Psi_{zz} + \Psi_z[\Psi_z - r \Psi_{rz}] - r^3 P_r + \frac{1}{Re}[(r - \alpha r^3) \Psi_{rz} - r^2 \Psi_{zrr} - r^2 \Psi_{zzz}] = 0, \tag{2.11}$$

where $Re \equiv aV/\nu$ is the cross-flow Reynolds number. Note that Re is positive for injection and negative for suction.

The wall permeance or injection coefficient A is defined as $A = Re/\alpha$, it is a measure of wall permeability.

From (2.6) and (2.9), we can write

$$u = \frac{1}{r} \frac{\partial \Psi}{\partial r}, \quad v = -\frac{1}{r} \frac{\partial \Psi}{\partial z}. \tag{2.12}$$

The boundary conditions (2.4) will be

$$\begin{aligned} &\text{(i)}\ \Psi_r = 0, \quad \psi_z = 1 \quad \text{at } r = 1, \\ &\text{(ii)}\ \left(\frac{\Psi_r}{r}\right)_r = 0, \quad \Psi_z = 0 \quad \text{at } r = 0, \\ &\text{(iii)}\ \psi_r = 0 \quad \text{at } z = 0. \end{aligned} \tag{2.13}$$

From a physical standpoint, our idealization is based on a decelerating expansion rate that follows a plausible model according to which

$$a\dot{a} = \text{constant}. \tag{2.14}$$

So, the rate of expansion decreases as the internal radius increases.

Since $\alpha = a\dot{a}/\nu$, then, integration of (2.14) yields

$$\frac{a}{a_0} = \sqrt{1 + \frac{2\alpha\nu t}{a_0^2}}, \tag{2.15}$$

where a_0 is the initial value of the radius.

3. Solution of the problem

Firstly, we shall derive the similarity solutions using the Lie group method under which (2.10) and (2.11) are invariant.

3.1. Lie point symmetries

Consider the one-parameter (ε) Lie group of infinitesimal transformations in $(z, r, \bar{t}, \Psi, P)$ given by

$$\begin{aligned}
z^* &= z + \varepsilon\phi(z, r, \bar{t}, \Psi, P) + \mathrm{O}(\varepsilon^2),\\
r^* &= r + \varepsilon\zeta(z, r, \bar{t}, \Psi, P) + \mathrm{O}(\varepsilon^2),\\
t^* &= \bar{t} + \varepsilon F(z, r, \bar{t}, \Psi, P) + \mathrm{O}(\varepsilon^2),\\
\Psi^* &= \Psi + \varepsilon\eta(z, r, \bar{t}, \Psi, P) + \mathrm{O}(\varepsilon^2),\\
P^* &= P + \varepsilon g(z, r, \bar{t}, \Psi, P) + \mathrm{O}(\varepsilon^2),
\end{aligned} \tag{3.1}$$

where "ε" is a small parameter.

A system of partial differential equations (2.10) and (2.11) is said to admit a symmetry generated by the vector field

$$X \equiv \phi\frac{\partial}{\partial z} + \zeta\frac{\partial}{\partial r} + F\frac{\partial}{\partial \bar{t}} + \eta\frac{\partial}{\partial \Psi} + g\frac{\partial}{\partial P}, \tag{3.2}$$

if it is left invariant by the transformation $(z, r, \bar{t}, \Psi, P) \to (z^*, r^*, t^*, \Psi^*, P^*)$.

Equivalently, we can obtain $(z^*, r^*, t^*, \Psi^*, P^*)$ by solving

$$\begin{aligned}
&\frac{\mathrm{d}z^*}{\mathrm{d}\varepsilon} = \phi(z^*, r^*, t^*, \Psi^*, P^*), \quad \frac{\mathrm{d}r^*}{\mathrm{d}\varepsilon} = \zeta(z^*, r^*, t^*, \Psi^*, P^*), \quad \frac{\mathrm{d}t^*}{\mathrm{d}\varepsilon} = F(z^*, r^*, t^*, \Psi^*, P^*),\\
&\frac{\mathrm{d}\Psi^*}{\mathrm{d}\varepsilon} = \eta(z^*, r^*, t^*, \Psi^*, P^*), \quad \frac{\mathrm{d}P^*}{\mathrm{d}\varepsilon} = g(z^*, r^*, t^*, \Psi^*, P^*),
\end{aligned} \tag{3.3}$$

subjected to the initial conditions

$$(z^*, r^*, t^*, \Psi^*, P^*)|_{\varepsilon=0} \equiv (z, r, \bar{t}, \Psi, P). \tag{3.4}$$

The solutions $\Psi = \Psi(z, r, \bar{t})$ and $P = P(z, r, \bar{t})$ are invariant under symmetry (3.2) if

$$\Phi_\Psi = X(\Psi - \Psi(z, r, \bar{t})) = 0 \quad \text{when } \Psi = \Psi(z, r, \bar{t}) \tag{3.5}$$

and

$$\Phi_P = X(P - P(z, r, \bar{t})) = 0 \quad \text{when } P = P(z, r, \bar{t}). \tag{3.6}$$

These conditions can be expressed by using the characteristic of the group, which are

$$\Phi_\Psi = \eta - \phi\frac{\partial\Psi}{\partial z} - \zeta\frac{\partial\Psi}{\partial r} - F\frac{\partial\Psi}{\partial \bar{t}} - g\frac{\partial\Psi}{\partial P} \tag{3.7}$$

and

$$\Phi_P = g - \phi\,\frac{\partial P}{\partial z} - \zeta\,\frac{\partial P}{\partial r} - F\,\frac{\partial P}{\partial \bar{t}} - \eta\,\frac{\partial P}{\partial \Psi}. \tag{3.8}$$

From (3.5)–(3-6), the solutions $\Psi = \Psi(z, r, \bar{t})$ and $P = P(z, r, \bar{t})$ are invariant provided that

$$\Phi_\Psi = 0 \quad \text{when } \Psi = \Psi(z, r, \bar{t}) \tag{3.9}$$

and

$$\Phi_P = 0 \quad \text{when } P = P(z, r, \bar{t}). \tag{3.10}$$

Thus, (3.7) and (3.8) can be rewritten as,

$$\phi\,\frac{\partial \Psi}{\partial z} + \zeta\,\frac{\partial \Psi}{\partial r} + F\,\frac{\partial \Psi}{\partial \bar{t}} + g\,\frac{\partial \Psi}{\partial P} = \eta, \tag{3.11}$$

$$\phi\,\frac{\partial P}{\partial z} + \zeta\,\frac{\partial P}{\partial r} + F\,\frac{\partial P}{\partial \bar{t}} + \eta\,\frac{\partial P}{\partial \Psi} = g. \tag{3.12}$$

Eqs. (3.11) and (3.12) are called the invariant surface conditions, which are quasilinear equations.

The subsidiary equations may be written as

$$\frac{\mathrm{d}z}{\phi(z, r, \bar{t}, \Psi, P)} = \frac{\mathrm{d}r}{\zeta(z, r, \bar{t}, \Psi, P)} = \frac{\mathrm{d}\bar{t}}{F(z, r, \bar{t}, \Psi, P)} = \frac{\mathrm{d}\Psi}{\eta(z, r, \bar{t}, \Psi, P)} = \frac{\mathrm{d}P}{g(z, r, \bar{t}, \Psi, P)}. \tag{3.13}$$

To calculate the prolongation of a given transformation, we need to differentiate (3.1) with respect to each of the variables, z, r and $\bar{t}$. To do this, we introduce the following total derivatives:

$$\begin{aligned}
D_z &\equiv \partial_z + \Psi_z \partial_\Psi + P_z \partial_P + \Psi_{zz}\partial_{\Psi_z} + P_{zz}\partial_{P_z} + \Psi_{zr}\partial_{\Psi_r} + \cdots,\\
D_r &\equiv \partial_r + \Psi_r \partial_\Psi + P_r \partial_P + \Psi_{rr}\partial_{\Psi_r} + P_{rr}\partial_{P_r} + \Psi_{zr}\partial_{\Psi_z} + \cdots,\\
D_{\bar{t}} &\equiv \partial_{\bar{t}} + \Psi_{\bar{t}} \partial_\Psi + P_{\bar{t}} \partial_P + \Psi_{\bar{t}\bar{t}}\partial_{\Psi_{\bar{t}}} + P_{\bar{t}\bar{t}}\partial_{P_{\bar{t}}} + \Psi_{z\bar{t}}\partial_{\Psi_z} + \cdots,
\end{aligned} \tag{3.14}$$

A vector X given by (3.2) is said to be a Lie point symmetry vector field for (2.10) and (2.11) if

$$\begin{aligned}
&X^{[3]}(r^2\Psi_{r\bar{t}} + r\Psi_r\Psi_{rz} + \Psi_z[\Psi_r - r\Psi_{rr}] + r^3 P_z\\
&\quad + \frac{1}{Re}[(r - \alpha r^3)\Psi_{rr} - r^2\Psi_{rrr} - r^2\Psi_{rzz} - (1 + \alpha r^2)\Psi_r]) = 0
\end{aligned} \tag{3.15}$$

and

$$X^{[3]}(r^2\Psi_{z\bar{t}} + r\Psi_r\Psi_{zz} + \Psi_z[\Psi_z - r\Psi_{rz}] - r^3 P_r + \frac{1}{Re}[(r - \alpha r^3)\Psi_{rz} - r^2\Psi_{zrr} - r^2\Psi_{zzz}]) = 0, \tag{3.16}$$

where

$$\begin{aligned}
X^{[3]} \equiv{}& \phi\,\frac{\partial}{\partial z} + \zeta\,\frac{\partial}{\partial r} + F\,\frac{\partial}{\partial \bar{t}} + \eta\,\frac{\partial}{\partial \Psi} + g\,\frac{\partial}{\partial P} + \eta^z\,\frac{\partial}{\partial \Psi_z} + \eta^r\,\frac{\partial}{\partial \Psi_r} + g^z\,\frac{\partial}{\partial P_z} + g^r\,\frac{\partial}{\partial P_r} + \eta^{rz}\,\frac{\partial}{\partial \Psi_{rz}} + \eta^{r\bar{t}}\,\frac{\partial}{\partial \Psi_{r\bar{t}}}\\
&+ \eta^{z\bar{t}}\,\frac{\partial}{\partial \Psi_{z\bar{t}}} + \eta^{zz}\,\frac{\partial}{\partial \Psi_{zz}} + \eta^{rr}\,\frac{\partial}{\partial \Psi_{rr}} + \eta^{rzz}\,\frac{\partial}{\partial \Psi_{rzz}} + \eta^{zrr}\,\frac{\partial}{\partial \Psi_{zrr}} + \eta^{zzz}\,\frac{\partial}{\partial \Psi_{zzz}} + \eta^{rrr}\,\frac{\partial}{\partial \Psi_{rrr}}
\end{aligned} \tag{3.17}$$

is the third prolongation of X.

The components $\eta^z, \eta^r, g^z, g^r, \eta^{rz}, \eta^{r\bar{t}}, \eta^{z\bar{t}}, \eta^{zz}, \eta^{rr}, \eta^{rzz}, \eta^{zrr}, \eta^{zzz}, \eta^{rrr}$ can be determined from the following expressions:

$$\begin{aligned}
&\eta^S = D_S\eta - \Psi_z D_S\phi - \Psi_r D_S\zeta - \Psi_{\bar{t}} D_S F, \quad g^N = D_N g - P_z D_N\phi - P_r D_N\zeta - P_{\bar{t}} D_N F,\\
&\eta^{JS} = D_S\eta^J - \Psi_{Jz} D_S\phi - \Psi_{Jr} D_S\zeta - \Psi_{J\bar{t}} D_S F,
\end{aligned} \tag{3.18}$$

where S, J stand for $z, r, \bar{t}$ and N stands for z, r.

Substituting (3.18) into (3.15), and using (2.10) and (2.11) to eliminate P_z and P_r , will lead to a large expression; then, equating to zero the coefficients of $\Psi_{\bar{t}\bar{t}}$, $\Psi_r\Psi_{\bar{t}\bar{t}}$, $\Psi_{r\bar{t}}\Psi_{\bar{t}\bar{t}}$, Ψ_{zzzzz}, $\Psi_z\Psi_{zzzzz}$, $\Psi_r\Psi_{zzzzz}$ and $\Psi_{zr\bar{t}}$ gives

$$F_r = F_\Psi = F_P = \eta_P = \phi_P = \zeta_P = F_z = 0. \tag{3.19}$$

Substituting (3.19) into (3.15) will remove many terms. Then, equating to zero the coefficients of $\Psi_r\Psi_{zzz}$, $(\Psi_{rz})^2$, $\Psi_r\Psi_{\bar{t}}$ and $\Psi_{\bar{t}}$ gives

$$\phi_\Psi = \zeta_\Psi = \eta_{\Psi\Psi} = \eta_{r\Psi} = 0. \tag{3.20}$$

Substituting (3.20) into (3.15), from (3.19) and (3.20) into (3.16), leads to a system of determining equations [1–3,5–7,9–11,13,16]. Solving the determining equations, we get

$$\phi = C_1(\bar{t}), \quad \zeta = 0, \quad F = C_2, \quad \eta = \frac{r^2}{2}C_1'(\bar{t}) + C_3(\bar{t}), \quad g = (2\alpha K C_1'(\bar{t}) - C_1''(\bar{t}))z + C_4(\bar{t}), \tag{3.21}$$

where $K = 1/Re$.

The invariance of boundary conditions (2.13) yields

$$C_1(\bar{t}) = C_1. \tag{3.22}$$

Substituting (3.22) into (3.21) gives

$$\phi = C_1, \quad \zeta = 0, \quad F = C_2, \quad \eta = C_3(\bar{t}), \quad g = C_4(\bar{t}). \tag{3.23}$$

The system of nonlinear equations (2.10)–(2.11) has the four-parameter Lie group of point symmetries generated by

$$X_1 \equiv \frac{\partial}{\partial z}, \quad X_2 \equiv \frac{\partial}{\partial \bar{t}}, \quad X_3 \equiv C_3(\bar{t})\frac{\partial}{\partial \Psi}, \quad X_4 \equiv C_4(\bar{t})\frac{\partial}{\partial P}. \tag{3.24}$$

The one-parameter group generated by X_1 and X_2 consists of translations, whereas the remaining symmetries X_3 and X_4 are nontrivial.

The commutator table of the symmetries is given below, where the entry in the ith row and jth column is defined as $[X_i, X_j] = X_iX_j - X_jX_i$, see Table 1.

The finite transformations corresponding to the symmetries X_1 to X_4 are, respectively,

$$\begin{aligned}
&X_1\colon\ z^* = z + \varepsilon_1, \quad r^* = r, \quad t^* = \bar{t}, \quad \Psi^* = \Psi, \quad P^* = P,\\
&X_2\colon\ z^* = z, \quad r^* = r, \quad t^* = \bar{t} + \varepsilon_2, \quad \Psi^* = \Psi, \quad P^* = P,\\
&X_3\colon\ z^* = z, \quad r^* = r, \quad t^* = \bar{t}, \quad \Psi^* = \Psi + \varepsilon_3 C_3(\bar{t}), \quad P^* = P,\\
&X_4\colon\ z^* = z, \quad r^* = r, \quad t^* = \bar{t}, \quad \Psi^* = \Psi, \quad P^* = P + \varepsilon_4 C_4(\bar{t}),
\end{aligned} \tag{3.25}$$

where ε_1 to ε_4 are group parameters.

For X_3, the characteristic

$$\Phi = (\Phi_\Psi, \Phi_P) \tag{3.26}$$

has the components

$$\Phi_\Psi = C_3(\bar{t}), \quad \Phi_P = 0. \tag{3.27}$$

Therefore, no solutions are invariant under the group generated by X_3.

For X_4, the characteristic (3.26) has the components

$$\Phi_\Psi = 0, \quad \Phi_P = C_4(\bar{t}). \tag{3.28}$$

Therefore, no solutions are invariant under the group generated by X_4.

Table 1
Table of commutators of the basis operators

	X_1	X_2	$X_3(C_3)$	$X_4(C_4)$
X_1	0	0	0	0
X_2	0	0	$X_3(C_3')$	$X_4(C_4')$
$X_3(C_3)$	0	$-X_3(C_3')$	0	0
$X_4(C_4)$	0	$-X_4(C_4')$	0	0

For X_1, the characteristic (3.26) has the components

$$\Phi_\Psi = -\Psi_z, \quad \Phi_P = -P_z. \tag{3.29}$$

Therefore, the general solutions of the invariant surface conditions (3.9) and (3.10) are

$$\Psi \equiv \Psi(r, \bar{t}), \quad P \equiv P(r, \bar{t}). \tag{3.30}$$

From (3.30) into (2.12), we get

$$u = u(r, \bar{t}), \quad v = 0. \tag{3.31}$$

Eq. (3.31) is a solution of the continuity equation (2.1) and momentum equation (2.2), even though it is not a particularly interesting one since it contradicts the boundary conditions.

For X_2, the characteristic (3.26) has the components

$$\Phi_\Psi = -\Psi_{\bar{t}}, \quad \Phi_P = -P_{\bar{t}}. \tag{3.32}$$

Therefore, the general solutions of the invariant surface conditions (3.9) and (3.10) are

$$\begin{aligned} \Psi &= h(r)H(z, r), \\ P &= \Gamma(z, r). \end{aligned} \tag{3.33}$$

Substituting (3.33) into (2.10) yields

$$\begin{aligned} &-r^2K\frac{\mathrm{d}^3h}{\mathrm{d}r^3} + \left[-rhH_z + Kr - \alpha Kr^3 - 3Kr^2\frac{H_r}{H}\right]\frac{\mathrm{d}^2h}{\mathrm{d}r^2} \\ &+ \left[hH_z - rh\frac{H_zH_r}{H} + 2K(r-\alpha r^3)\frac{H_r}{H} - 3Kr^2\frac{H_{rr}}{H} - Kr^2\frac{H_{zz}}{H} - K - \alpha Kr^2 + rhH_{rz}\right]\frac{\mathrm{d}h}{\mathrm{d}r} \\ &+ rH_z\left(\frac{\mathrm{d}h}{\mathrm{d}r}\right)^2 + \left[K(r-\alpha r^3)\frac{H_{rr}}{H} - Kr^2\frac{H_{rrr}}{H} - Kr^2\frac{H_{rzz}}{H} - K(1+\alpha r^2)\frac{H_r}{H}\right]h \\ &+ \left[r\frac{H_rH_{rz}}{H} + \frac{H_rH_z}{H} - r\frac{H_zH_{rr}}{H}\right]h^2 + \frac{r^3}{H}\frac{\partial\Gamma}{\partial z} = 0, \end{aligned} \tag{3.34}$$

which can be rewritten as

$$\begin{aligned} &-r^2K\frac{\mathrm{d}^3h}{\mathrm{d}r^3} + [-rhK_1 + Kr - \alpha Kr^3 - 3Kr^2K_2]\frac{\mathrm{d}^2h}{\mathrm{d}r^2} \\ &+ [hK_1 - rhK_3 + 2K(r-\alpha r^3)K_2 - 3Kr^2K_5 - Kr^2K_4 - K - \alpha Kr^2 + rhK_8]\frac{\mathrm{d}h}{\mathrm{d}r} + rK_1\left(\frac{\mathrm{d}h}{\mathrm{d}r}\right)^2 \\ &+ [K(r-\alpha r^3)K_5 - Kr^2K_7 - Kr^2K_6 - K(1+\alpha r^2)K_2]h + [rK_9 + K_3 - rK_{10}]h^2 + \frac{r^3}{H}\frac{\partial\Gamma}{\partial z} = 0, \end{aligned} \tag{3.35}$$

where

$$K_1 = H_z, \quad K_2 = \frac{H_r}{H}, \quad K_3 = \frac{H_z H_r}{H}, \quad K_4 = \frac{H_{zz}}{H}, \quad K_5 = \frac{H_{rr}}{H}, \quad K_6 = \frac{H_{rzz}}{H}, \quad K_7 = \frac{H_{rrr}}{H},$$

$$K_8 = H_{rz}, \quad K_9 = \frac{H_r H_{rz}}{H}, \quad K_{10} = \frac{H_z H_{rr}}{H}. \tag{3.36}$$

Since h is a function of r only, whereas H and Γ are functions of z and r, thus from Eq. (3.35) we conclude that each of K_i, $i = 1, 2, \ldots, 10$, must be a constant or function of r only to obtain an expression in the single variable r.

Solution of $H_z = K_1$ in (3.36) gives

$$H(z, r) = zK_1(r) + K_{11}(r). \tag{3.37}$$

Substituting (3.37) into (3.33) will give

$$\Psi = (zK_1(r) + K_{11}(r))h(r). \tag{3.38}$$

Differentiation of (3.38) with respect to r, and using (2.13)(iii), yields

$$K_{11}(r)h(r) = K_{12}, \tag{3.39}$$

where K_{12} is constant.

Substituting (3.39) into (3.38) gives

$$\Psi = zG(r) + K_{12}, \tag{3.40}$$

where

$$G(r) = K_1(r)h(r). \tag{3.41}$$

Substitution from the second equation of (3.33) and (3.40) into (2.10) yields

$$r^3 \frac{\partial \Gamma}{\partial z} = z\left[r^2 K \frac{\mathrm{d}^3 G}{\mathrm{d}r^3} + (rG - (r - \alpha r^3)K)\frac{\mathrm{d}^2 G}{\mathrm{d}r^2} + ((1 + \alpha r^2)K - G)\frac{\mathrm{d}G}{\mathrm{d}r} - r\left(\frac{\mathrm{d}G}{\mathrm{d}r}\right)^2\right]. \tag{3.42}$$

Substituting (3.37) and (3.42) into the last term of (3.35) yields

$$K_{11} = 0. \tag{3.43}$$

Substituting (3.43) into (3.37), we get

$$H(z, r) = zK_1(r), \tag{3.44}$$

which satisfies the remaining K_j, $j = 2, \ldots, 10$.

Substituting (3.43) into (3.39), then into (3.40), we get

$$\Psi = zG(r). \tag{3.45}$$

Using (3.45) in (2.12), we get

$$u = \frac{z}{r}\frac{\mathrm{d}G}{\mathrm{d}r}, \quad v = -\frac{G}{r}. \tag{3.46}$$

Substituting (3.45) into (2.11) and then differentiating with respect to z yields

$$P_{rz} = 0. \tag{3.47}$$

Using (3.45) into (2.10), then differentiating with respect to r and using (3.47), we get

$$K\left[r^2 \frac{\mathrm{d}^4 G}{\mathrm{d}r^4} + (\alpha r^3 - 2r)\frac{\mathrm{d}^3 G}{\mathrm{d}r^3} + (\alpha r^2 + 3)\frac{\mathrm{d}^2 G}{\mathrm{d}r^2} - \left(\alpha r + \frac{3}{r}\right)\frac{\mathrm{d}G}{\mathrm{d}r}\right] - r\frac{\mathrm{d}G}{\mathrm{d}r}\frac{\mathrm{d}^2 G}{\mathrm{d}r^2} + \left(\frac{\mathrm{d}G}{\mathrm{d}r}\right)^2$$

$$- 3G\frac{\mathrm{d}^2 G}{\mathrm{d}r^2} + \frac{3}{r}G\frac{\mathrm{d}G}{\mathrm{d}r} + rG\frac{\mathrm{d}^3 G}{\mathrm{d}r^3} = 0. \tag{3.48}$$

For simplification, let

$$\beta \equiv \frac{r^2}{2}. \tag{3.49}$$

Eq. (3.48) will take the form

$$K\left[2\beta\frac{\mathrm{d}^4G}{\mathrm{d}\beta^4} + (2\alpha\beta+4)\frac{\mathrm{d}^3G}{\mathrm{d}\beta^3} + 4\alpha\frac{\mathrm{d}^2G}{\mathrm{d}\beta^2}\right] + G\,\frac{\mathrm{d}^3G}{\mathrm{d}\beta^3} - \frac{\mathrm{d}G}{\mathrm{d}\beta}\,\frac{\mathrm{d}^2G}{\mathrm{d}\beta^2} = 0. \tag{3.50}$$

The boundary conditions (2.13) will be

$$\text{(i)}\ \frac{\mathrm{d}G(1/2)}{\mathrm{d}\beta} = 0, \quad \text{(ii)}\ G(\tfrac{1}{2}) = 1, \quad \text{(iii)}\ G(0) = 0, \quad \text{(iv)}\ \lim_{\beta\to 0}\sqrt{2\beta}\,\frac{\mathrm{d}^2G}{\mathrm{d}\beta^2} = 0. \tag{3.51}$$

3.2. Analytical solution

The fourth-order, nonlinear differential equation (3.50) with the boundary conditions (3.51) is solved using small-parameter perturbations [14,15].

First, assume

$$G = G_1 + KG_2 + \mathrm{O}(K^2). \tag{3.52}$$

Substituting (3.52) into (3.50), the leading order term will be

$$G_1\,\frac{\mathrm{d}^3G_1}{\mathrm{d}\beta^3} - \frac{\mathrm{d}G_1}{\mathrm{d}\beta}\,\frac{\mathrm{d}^2G_1}{\mathrm{d}\beta^2} = 0, \tag{3.53}$$

with the boundary conditions

$$\text{(i)}\ \frac{\mathrm{d}G_1(1/2)}{\mathrm{d}\beta} = 0, \quad \text{(ii)}\ G_1(\tfrac{1}{2}) = 1, \quad \text{(iii)}\ G_1(0) = 0, \quad \text{(iv)}\ \lim_{\beta\to 0}\sqrt{2\beta}\,\frac{\mathrm{d}^2G_1}{\mathrm{d}\beta^2} = 0. \tag{3.54}$$

Solution of (3.53) with the boundary conditions (3.54) gives

$$G_1 = \sin\,\theta, \tag{3.55}$$

where

$$\theta = \pi\beta. \tag{3.56}$$

The first-order term will be

$$2\,\beta\frac{\mathrm{d}^4G_1}{\mathrm{d}\beta^4} + (2\alpha\beta+4)\frac{\mathrm{d}^3G_1}{\mathrm{d}\beta^3} + 4\alpha\,\frac{\mathrm{d}^2G_1}{\mathrm{d}\beta^2} + G_1\,\frac{\mathrm{d}^3G_2}{\mathrm{d}\beta^3} + G_2\,\frac{\mathrm{d}^3G_1}{\mathrm{d}\beta^3} - \frac{\mathrm{d}G_1}{\mathrm{d}\beta}\,\frac{\mathrm{d}^2G_2}{\mathrm{d}\beta^2} - \frac{\mathrm{d}G_2}{\mathrm{d}\beta}\,\frac{\mathrm{d}^2G_1}{\mathrm{d}\beta^2} = 0, \tag{3.57}$$

with the boundary conditions

$$\text{(i)}\ \frac{\mathrm{d}G_2(\frac{1}{2})}{\mathrm{d}\beta} = 0, \quad \text{(ii)}\ G_2(\tfrac{1}{2}) = 0, \quad \text{(iii)}\ G_2(0) = 0, \quad \text{(iv)}\ \lim_{\beta\to 0}\sqrt{2\beta}\,\frac{\mathrm{d}^2G_2}{\mathrm{d}\beta^2} = 0. \tag{3.58}$$

Substituting (3.55) and (3.56) into (3.57) and (3.58), we get

$$\sin\theta\,\frac{\mathrm{d}^3G_2}{\mathrm{d}\theta^3} - \cos\theta\,\frac{\mathrm{d}^2G_2}{\mathrm{d}\theta^2} + \sin\theta\,\frac{\mathrm{d}G_2}{\mathrm{d}\theta} - \cos\theta G_2 = \left(\frac{2}{\pi}\alpha\theta + 4\right)\cos\theta + \frac{4}{\pi}\alpha\sin\theta - 2\theta\sin\theta, \tag{3.59}$$

with the boundary conditions

$$\text{(i)}\ \frac{\mathrm{d}G_2(\pi/2)}{\mathrm{d}\theta} = 0, \quad \text{(ii)}\ G_2(\pi/2) = 0, \quad \text{(iii)}\ G_2(0) = 0, \quad \text{(iv)}\ \lim_{\theta\to 0}\sqrt{\theta}\,\frac{\mathrm{d}^2G_2}{\mathrm{d}\theta^2} = 0. \tag{3.60}$$

We guess a solution for the homogenous part of Eq. (3.59) in the form

$$G_{2h} = \cos\theta. \tag{3.61}$$

Following [8], we use the variation of parameters approach to find the correction multiplier based on

$$G_{2h} = C(\theta)\cos\theta. \tag{3.62}$$

Substituting (3.62) into the homogenous part of (3.59) yields

$$C(\theta) = D_1 \tan\theta + D_2\theta + D_3. \tag{3.63}$$

Using (3.63) into (3.62), we get

$$G_{2h} = D_1 \sin\theta + D_2\theta\cos\theta + D_3\cos\theta. \tag{3.64}$$

Using the method of variation of parameters, we assume

$$G_2 = D_1(\theta)\sin\theta + D_2(\theta)\theta\cos\theta + D_3(\theta)\cos\theta. \tag{3.65}$$

$D_1(\theta)$, $D_2(\theta)$ and $D_3(\theta)$ can be determined from

$$\begin{pmatrix} \sin\theta & \theta\cos\theta & \cos\theta \\ \cos\theta & \cos\theta - \theta\sin\theta & -\sin\theta \\ -\sin\theta & -2\sin\theta - \theta\cos\theta & -\cos\theta \end{pmatrix} \begin{pmatrix} D_1' \\ D_2' \\ D_3' \end{pmatrix} = \begin{pmatrix} 0 \\ 0 \\ \left(\frac{2}{\pi}\alpha\theta + 4\right)\cot\theta + \frac{4}{\pi}\alpha - 2\theta \end{pmatrix}. \tag{3.66}$$

Then, solving system (3.66) and integrating with respect to θ, we get

$$\begin{aligned} D_1(\theta) &= \frac{\alpha}{\pi}[\cos\theta - \theta\sin\theta + 3\ \ln\ \tan(\theta/2) - \theta\,\mathrm{cosec}\theta] - \sin\theta - 2\,\mathrm{cosec}\,\theta - \theta\cos\theta - I_1 + b_1, \\ D_2(\theta) &= \frac{\alpha}{\pi}[\theta\,\mathrm{cosec}\,\theta - 3\ \ln\ \tan(\theta/2)] + 2\mathrm{cosec}\theta + I_1 + b_2, \\ D_3(\theta) &= \frac{\alpha}{\pi}[-\theta^2\mathrm{cosec}\,\theta - \theta\cos\theta - \sin\theta + 3I_1] + \theta\sin\theta - 2\theta\,\mathrm{cosec}\,\theta - \cos\theta - I_2 + b_3, \end{aligned} \tag{3.67}$$

where

$$I_1 = \int_0^\theta \theta\,\mathrm{cosec}\,\theta\,\mathrm{d}\theta, \quad I_2 = \int_0^\theta \theta^2\mathrm{cosec}\,\theta\,\mathrm{d}\theta \quad \text{and } b_1,\ b_2 \text{ and } b_3 \text{ are constants.}$$

Substituting (3.67) into (3.65), we get

$$G_2 = \begin{bmatrix} \frac{\alpha}{\pi}[3\ \ln\ \tan(\theta/2)(\sin\theta - \theta\cos\theta) - 2\theta] - 3 + (\theta\cos\theta - \sin\theta)I_1 \\ + \left(\frac{3\alpha}{\pi}I_1 - I_2\right)\cos\theta + b_1\sin\theta + b_2\theta\cos\theta + b_3\cos\theta \end{bmatrix}. \tag{3.68}$$

Using (3.68) and (3.55) into (3.52) yields

$$G = \sin\theta + K\begin{bmatrix} \frac{\alpha}{\pi}[3\ \ln\ \tan(\theta/2)(\sin\theta - \theta\cos\theta) - 2\theta] - 3 + (\theta\cos\theta - \sin\theta)I_1 \\ + \left(\frac{3\alpha}{\pi}I_1 - I_2\right)\cos\theta + b_1\sin\theta + b_2\theta\cos\theta + b_3\cos\theta \end{bmatrix}, \tag{3.69}$$

with boundary conditions

$$\text{(i)}\ \frac{\mathrm{d}G(\pi/2)}{\mathrm{d}\theta} = 0, \quad \text{(ii)}\ G(\pi/2) = 1, \quad \text{(iii)}\ G(0) = 0, \quad \text{(iv)}\ \lim_{\theta\to 0}\sqrt{\theta}\frac{\mathrm{d}^2G}{\mathrm{d}\theta^2} = 0. \tag{3.70}$$

Using (3.70) into (3.69), we get

$$b_1 = \alpha + 3 + I_1(\pi/2), \tag{3.71}$$

$$b_2 = -\frac{6}{\pi} + \left[\frac{2\alpha}{\pi^2} - 1\right] - \left[1 + \frac{6\alpha}{\pi^2}\right] I_1(\pi/2) + \frac{2}{\pi} I_2(\pi/2), \tag{3.72}$$

$$b_3 = 3. \tag{3.73}$$

The integrals I_1 and I_2 can be written in series form as

$$I_1(\theta) \cong \theta + \frac{\theta^3}{18} - \left[\frac{1}{5!} + \frac{1}{(3!)^2}\right]\frac{\theta^5}{5} + \left[\frac{1}{7!} + \frac{2}{(3!)(5!)} + \frac{1}{(3!)^3}\right]\frac{\theta^7}{7} - \left[\frac{1}{9!} + \frac{1}{(5!)^2} + \frac{2}{(3!)(7!)} + \frac{3}{(3!)^2 5!} + \frac{1}{(3!)^4}\right]\frac{\theta^9}{9} + \cdots, \tag{3.74}$$

$$I_2(\theta) \cong \frac{\theta^2}{2} + \frac{\theta^4}{24} - \left[\frac{1}{5!} + \frac{1}{(3!)^2}\right]\frac{\theta^6}{6} + \left[\frac{1}{7!} + \frac{2}{(3!)(5!)} + \frac{1}{(3!)^3}\right]\frac{\theta^8}{8} - \left[\frac{1}{9!} + \frac{1}{(5!)^2} + \frac{2}{(3!)(7!)} + \frac{3}{(3!)^2 5!} + \frac{1}{(3!)^4}\right]\frac{\theta^{10}}{10} + \cdots. \tag{3.75}$$

4. The velocity fields

In terms of β, Eq. (3.46) can be written as

$$u = zG_\beta, \quad v = -\frac{G}{\sqrt{2\beta}}. \tag{4.1}$$

4.1. Axial velocity

4.1.1. The effect of the wall expansion ratio α

Fig. 2 illustrates the behaviour of self-similar axial velocity u/z for cross-flow Reynolds numbers $Re = 100$, $Re = 500$ and $Re = 1000$, respectively, over a range of wall expansion ratio α. An initial glance indicates the greater sensitivity to wall expansion at $Re = 100$, see Fig. 2a. In case of expanding wall ($\alpha > 0$), the greater the α, that is, the expansion ratio of the wall is, the higher will be the axial velocity near the centre, and the lower near the wall. That is because the flow toward the centre becomes greater to make up for the space caused by the expansion of the wall and as a result the axial velocity also becomes greater near the centre. In case of contracting wall ($\alpha < 0$), increasing contraction ratio leads to lower axial velocity near the centre, and the higher near the wall because the flow toward the wall becomes greater and as a result the axial velocity near the wall becomes greater. The effect of suction on the self-similar axial velocity u/z over a range of wall expansion ratio α is illustrated in Fig. 3. The greater sensitivity to wall expansion appears at $Re = -100$, see Fig. 3a. In case of contracting wall, the greater the contraction ratio, that is, the higher the contraction velocity of the pipe wall, the higher the axial velocity will be near the centre, and the lower near the wall. In case of expanding wall, the greater the expansion ratio, that is, the higher the expanding velocity of the pipe wall, the lower the axial velocity will be near the centre, and the higher near the wall. Comparing analytical and numerical solutions, the results are found to be in very well agreement. As seen in Figs. 2 and 3, the largest error seems to occur near the centre. The injection solution with $Re = 100$ becomes less accurate with higher values of $|\alpha|$, especially with positive values of α (i.e., $\alpha = 50$). On the other hand, the suction solution with $Re = -100$ becomes more accurate with lower positive values of α, also with higher negative values of α, see Table 2. The magnified portions of the graphs indicate that the analytical and numerical solutions become indistinguishable in both cases, injection ($Re = 500$, $Re = 1000$) and suction ($Re = -500$, $Re = -1000$) each combined with contracting wall, while a small error appears with expanding wall, see Figs. 2b, c, 3b, c.

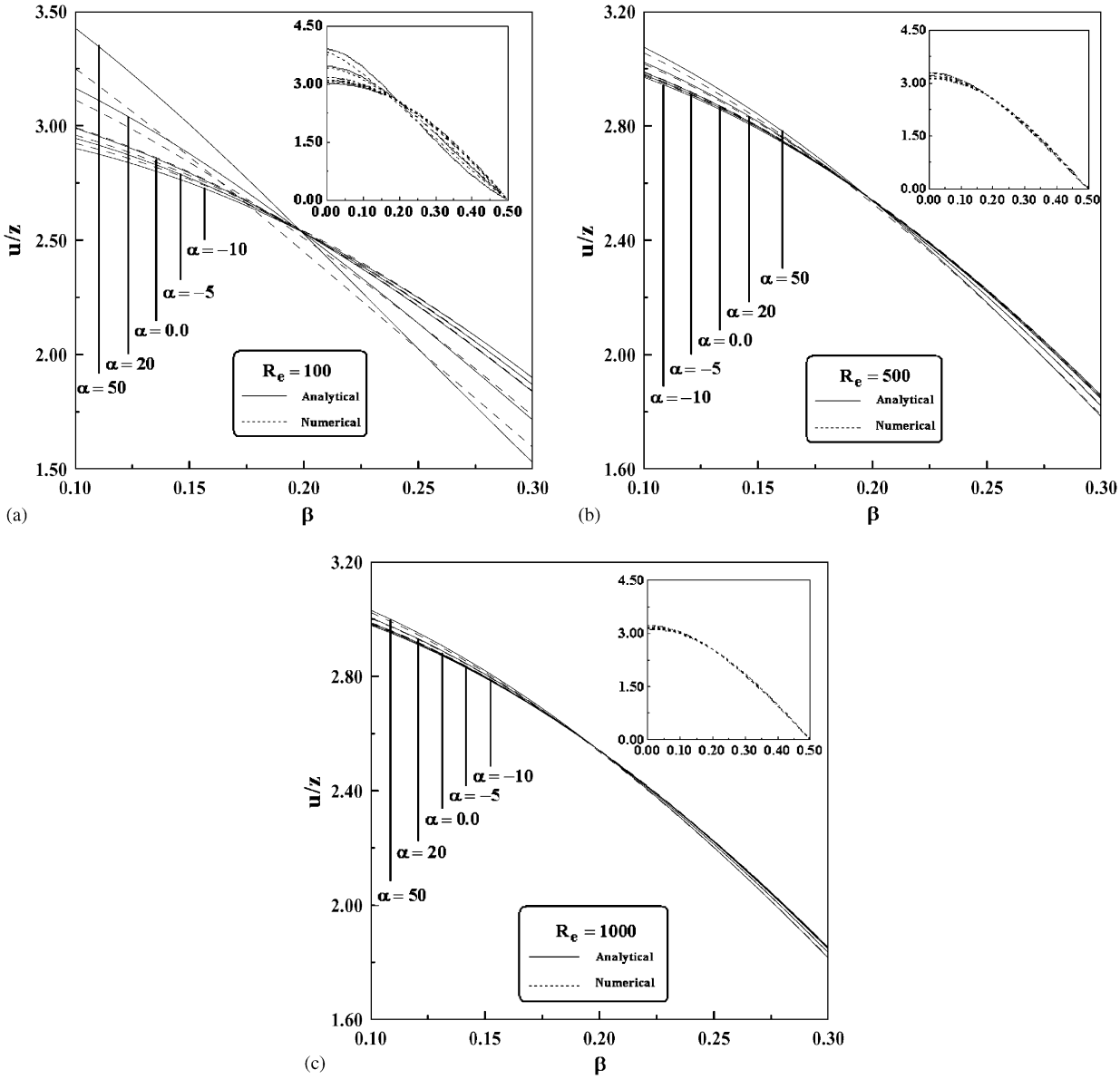

Fig. 2. Self-similar axial velocity profiles shown over a range of α at (a) $Re = 100$, (b) $Re = 500$ and (c) $Re = 1000$.

4.1.2. The effect of the cross-flow Reynolds number Re

Fig. 4 illustrates the behaviour of self-similar axial velocity u/z for wall expansion ratios $\alpha = 20$ and $\alpha = 50$, respectively, over a range of cross-flow Reynolds number Re. In case of injection, the percentage increase in self-similar axial velocity u/z at the centreline, as α varies from 20 to 50, at $Re = 100$ is very high compared with the percentage increase in case of $Re = 1000$. So, for smaller values of Re, the wall expansion is more sensitive than that for higher values of Re, which is due to the diminished role of viscosity at a higher Reynolds number, see Table 3. Similar conclusion can be made in case of suction, see Table 4. Also, the self-similar axial velocity near the centre increases as Re decreases in case of injection and it decreases as $|Re|$ decreases in case of suction. In case of contracting wall combined with both injection and suction, the behaviour of self-similar axial velocity u/z is illustrated in Fig. 5. The self-similar axial velocity u/z near the centre increases as Re increases in case of injection and it decreases as $|Re|$ increases in case of suction. The error between analytical and numerical solutions becomes noticeable in case of

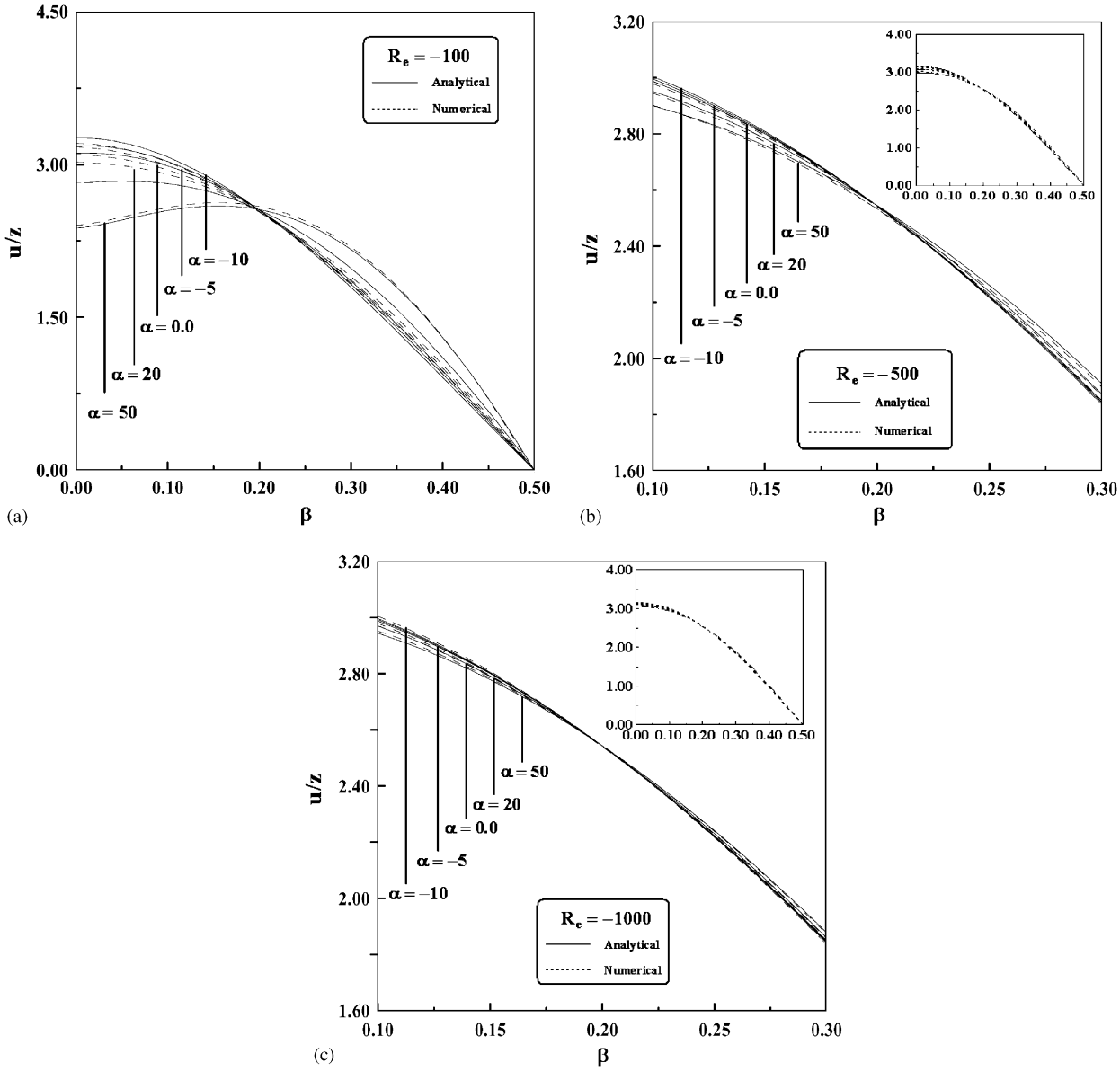

Fig. 3. Self-similar axial velocity profiles shown over a range of α at (a) $Re = -100$, (b) $Re = -500$ and (c) $Re = -1000$.

Table 2
Comparison between analytical and numerical solutions for self-similar axial velocity u/z at $\beta = 0.15$

u/z at $\beta = 0.15$	$Re = 100$		Percentage error (%)	$Re = -100$		Percentage error (%)
	Analytical	Numerical		Analytical	Numerical	
$\alpha = 50$	3.005369	2.901740	3.44813	2.592990	2.624850	1.22869
$\alpha = 20$	2.877895	2.838464	1.37013	2.720464	2.750422	1.10121
$\alpha = 0.0$	2.792913	2.796448	0.12657	2.805446	2.762831	1.51901
$\alpha = -5.0$	2.771667	2.781716	0.36256	2.826692	2.791586	1.24195
$\alpha = -10$	2.750422	2.765097	0.53355	2.847937	2.814923	1.15923

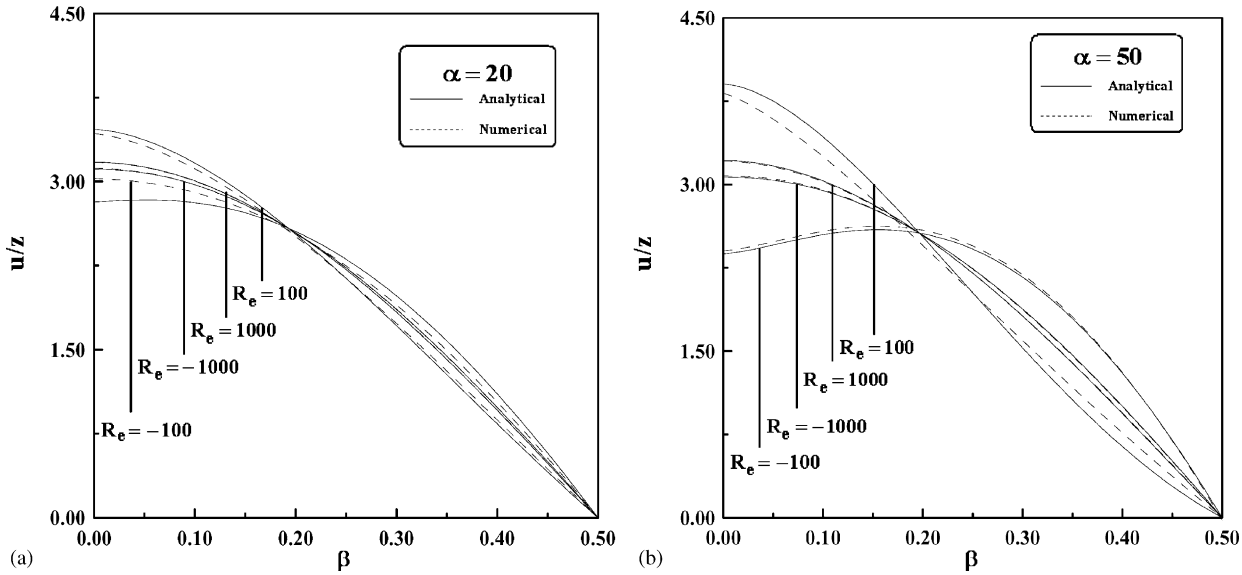

Fig. 4. Self-similar axial velocity profiles shown over a range of Re at (a) $\alpha = 20$ and (b) $\alpha = 50$.

Table 3
Comparison between the values of u/z at centreline in case of injection for different Re (analytical solution)

	$Re = 100$		$Re = 1000$	
	$\alpha = 20$	$\alpha = 50$	$\alpha = 20$	$\alpha = 50$
u/z	3.463053	3.907648	3.173737	3.218197

Table 4
Comparison between the values of u/z at centreline in case of suction for different Re (analytical solution)

	$Re = -100$		$Re = -1000$	
	$\alpha = 20$	$\alpha = 50$	$\alpha = 20$	$\alpha = 50$
u/z	2.816462	2.375538	3.109079	3.064987

$Re = 100$ and -100, especially with expanding wall, while analytical and numerical solutions in case of $Re = 1000$ and -1000 become indistinguishable in both cases, expanding and contracting wall, see Figs. 4 and 5.

4.2. Radial velocity

4.2.1. The effect of the wall expansion ratio α

Fig. 6 illustrates the behaviour of radial velocity v at different values of wall expansion ratio α for a fixed cross-flow Reynolds numbers $Re = 100$, 500 and 1000, respectively. The greater sensitivity to wall expansion appears at $Re = 100$, see Fig. 6a. In case of expanding wall, the radial velocity (absolute value) increases as α increases, while, in case of contracting wall, the radial velocity (absolute value) increases as $|\alpha|$ decreases. The effect of suction on the radial velocity v over a range of expansion ratio α is illustrated in Fig. 7. An initial glance indicates the greater sensitivity to wall expansion at $Re = -50$, see Fig. 7a. The higher the contraction velocity is, the greater the radial velocity (absolute value) will be. Hence, the radial velocity (absolute value) increases as α decreases. An interesting phenomenon is also

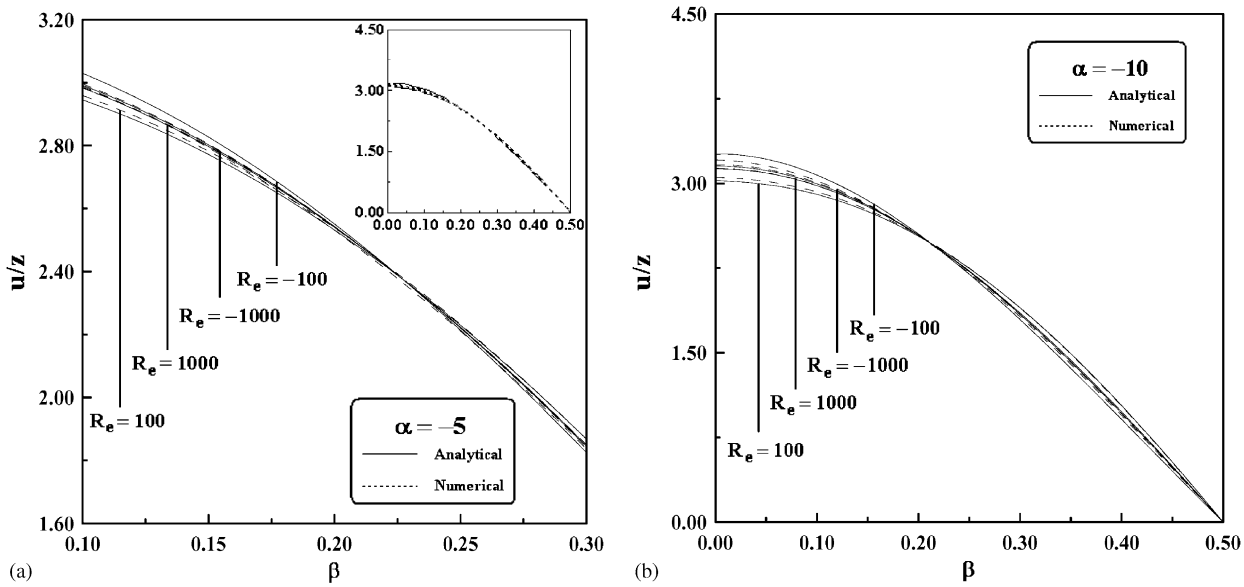

Fig. 5. Self-similar axial velocity profiles shown over a range of Re at (a) $\alpha = -5.0$ and (b) $\alpha = -10$.

observed in both cases of injection and suction, which is the existence of a point along the interval $0 < \beta < 0.5$, such that the radial velocity exceeds its (absolute) value at the wall. After this point, the radial velocity decreases until it reaches its value at the wall ($v = -1$) at $\beta = 0.5$. That is because the cylindrical flow area normal to the incoming streams is proportional to the radius, and the sudden reduction in it in the vicinity of the wall forces the radial velocity to increase (in absolute value) to keep satisfying mass conservation. Tables 5 and 6 indicate these points and the corresponding radial velocity overshoots relative to the wall.

As seen, the smallest overshoots (absolute value) with the closest distance to the wall in case of injection appears when wall expansion ratio is small enough (in case of expanding wall) or high enough (in case of contracting wall), see Table 5. While, in case of suction, the smallest overshoots (absolute value) with the closest distance to the wall appears when wall expansion ratio is high enough (in case of expanding wall) or low enough (in case of contracting wall), see Table 6. The error between analytical and numerical solutions becomes noticeable in case of $Re = 100$ with expanding wall ($\alpha = 50$), except this case, the results are found to be in excellent agreement, see Figs. 6 and 7.

4.2.2. *The effect of the cross-flow Reynolds number Re*

Fig. 8 illustrates the behaviour of radial velocity v at different values of cross-flow Reynolds number for fixed wall expansion $\alpha = 20$ and -10, respectively. In case of expanding wall combined with injection, the radial velocity increases (absolute value) with decreasing Re and it increases (absolute value) with increasing $|Re|$ in case of expanding wall combined with suction, see Fig. 8(a). Also, the radial velocity (absolute value) decreases with decreasing Re (contracting wall combined with injection) and it increases (absolute value) with decreasing $|Re|$ (contracting wall combined with suction), see Fig. 8b. Table 7 illustrates the comparison between the analytical and numerical solutions for radial velocity v at different values of cross-flow Reynolds number Re for dimensionless wall expansion ratio $\alpha = 20$ and $\alpha = -10$ at $\beta = 0.15$. In both cases, expanding wall with $\alpha = 20$ and contracting wall with $\alpha = -10$, the percentage error increases with decreasing Re (case of injection), while it decreases with increasing $|Re|$(case of suction), see Table 7.

The points that lie in the interval $0 < \beta < 0.5$, such that the radial velocity exceeds its value at the wall, are indicated in Table 8.

In case of expanding wall, the smallest overshoots (absolute value) with the closest distance to the wall appears when the cross-flow Reynolds number is high enough (in case of injection) or low enough (in case of suction), while, in case of contracting wall, the smallest overshoots (absolute value) with the closest distance to the wall appears when the cross-flow Reynolds number is low enough (in case of injection) or high enough (in case of suction), see Table 8.

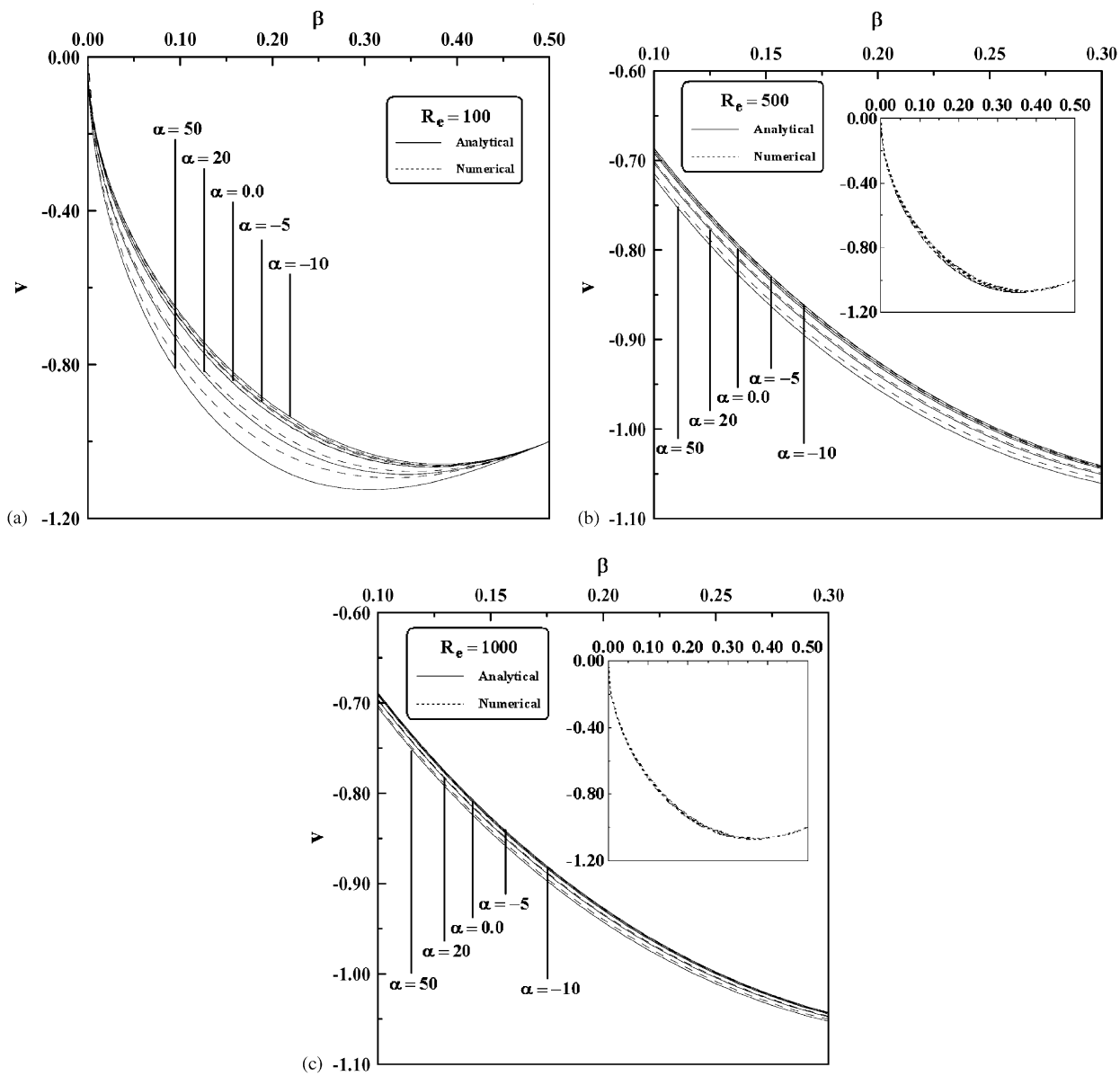

Fig. 6. Radial velocity profiles shown over a range of α at (a) $Re = 100$, (b) $Re = 500$ and (c) $Re = 1000$.

4.3. Flow streamlines

4.3.1. The effect of the wall expansion ratio α

Fig. 9 illustrates the streamlines at several discrete points along the length of the wall at different values of wall expansion ratio α for fixed cross-flow Reynolds numbers $Re = -50$ and 100, respectively. The suction pushes the streamlines away from the core closer to the wall, see Fig. 9a, while injection tends to push them closer to the core, see Fig. 9b. Differences in streamline curvatures and, hence, the flow turning speed become more appreciable in the downstream portions in both cases. A more gradual flow turning occurs when the walls are in the expansion mode in case of injection and in contraction mode in case of suction. As seen in Fig. 9, the fluid enters the wall almost perpendicular.

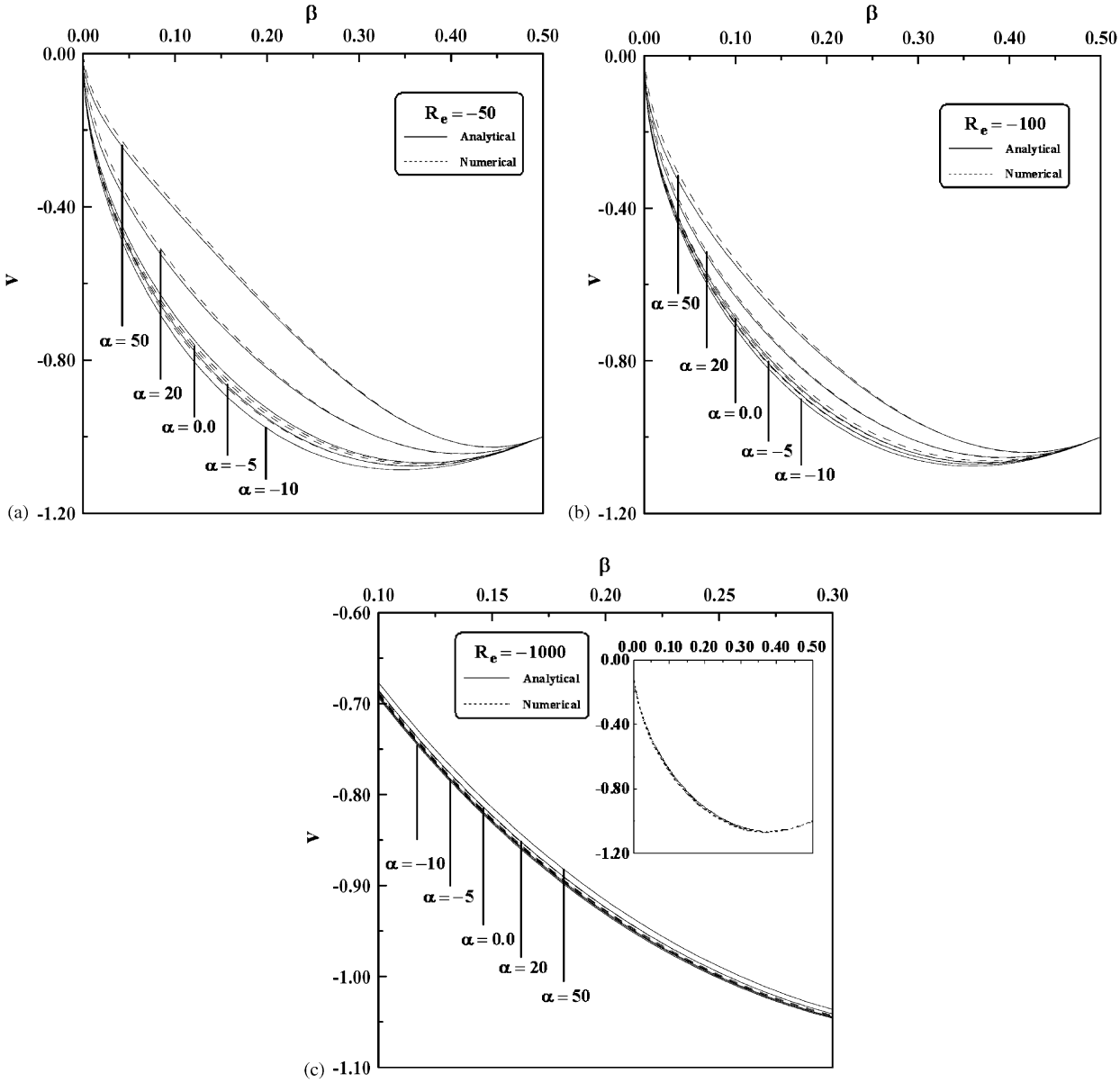

Fig. 7. Radial velocity profiles shown over a range of α at (a) $Re = -50$, (b) $Re = -100$ and (c) $Re = -1000$.

Table 5
Radial velocity overshoots relative to the wall in case of injection for different α (analytical solution)

	$Re = 100$		$Re = 500$		$Re = 1000$	
	r	v	r	v	r	v
$\alpha = 50$	0.78740	−1.125738	0.84853	−1.075596	0.84853	−1.070972
$\alpha = 20$	0.82462	−1.084838	0.86023	−1.07006	0.86023	−1.068464
$\alpha = 0.0$	0.86023	−1.066390	0.86023	−1.066753	0.86023	−1.066810
$\alpha = -5$	0.87178	−1.062324	0.86023	−1.065926	0.86023	−1.066397
$\alpha = -10$	0.87178	−1.058715	0.86023	−1.065099	0.86023	−1.065984

Table 6
Radial velocity overshoots relative to the wall in case of suction for different α (analytical solution)

	$Re = -50$		$Re = -100$		$Re = -1000$	
	r	v	r	v	r	v
$\alpha = 50$	0.93808	−1.027383	0.91652	−1.039776	0.87178	−1.062978
$\alpha = 20$	0.90554	−1.044215	0.88318	−1.053519	0.86023	−1.065272
$\alpha = 0.0$	0.86023	−1.068020	0.86023	−1.067444	0.86023	−1.066926
$\alpha = -5$	0.84853	−1.076798	0.86023	−1.071578	0.86023	−1.067339
$\alpha = -10$	0.83666	−1.086915	0.84853	−1.076252	0.86023	−1.067752

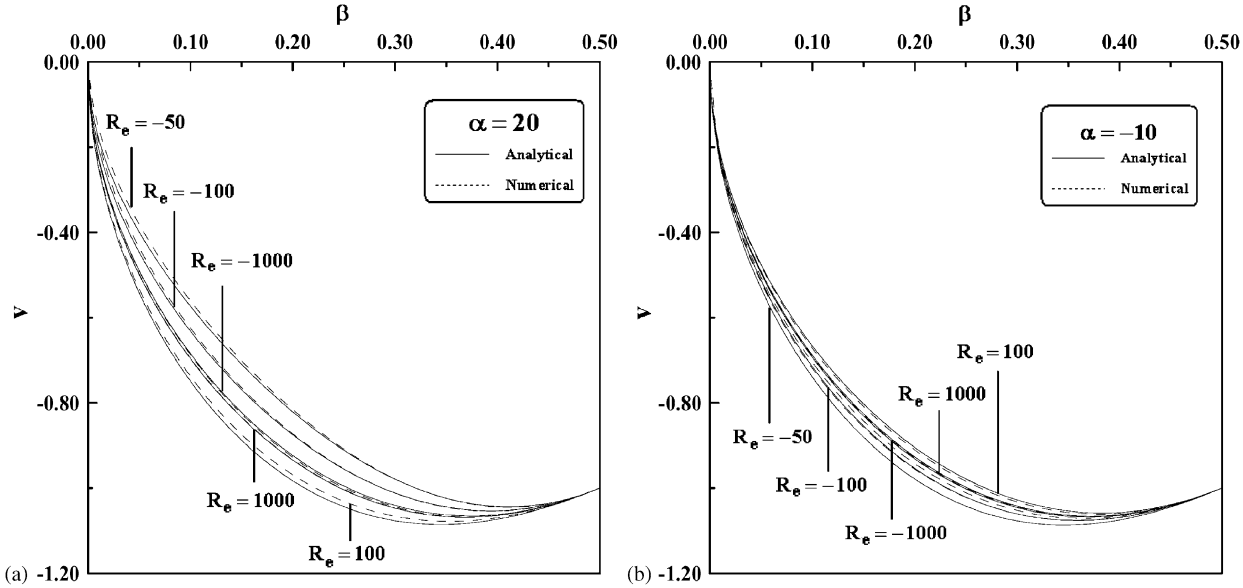

Fig. 8. Radial velocity profiles shown over a range of Re at (a) $\alpha = 20$ and (b) $\alpha = -10$.

Table 7
Comparison between analytical and numerical solutions for radial velocity v at $\beta = 0.15$

v at $\beta = 0.15$	$\alpha = 20$		Percentage error (%)	$\alpha = -10$		Percentage error (%)
	Analytical	Numerical		Analytical	Numerical	
$Re = 1000$	−0.834817	−0.833714	0.13212	−0.826263	−0.826609	0.04188
$Re = 100$	−0.888348	−0.874576	1.55029	−0.802806	−0.808874	0.75585
$Re = -50$	−0.709912	−0.701209	1.22593	−0.880996	−0.857874	2.62453
$Re = -100$	−0.769391	−0.764779	0.59944	−0.854933	−0.843372	1.35227
$Re = -1000$	−0.822922	−0.826419	0.42495	−0.831476	−0.829360	0.25449

4.3.2. The effect of the cross-flow Reynolds number Re

The effect of cross-flow Reynolds number on the streamlines for wall expansion ratios $\alpha = 20$ and -10, respectively, is illustrated in Fig. 10. As the Reynolds number decreases, the effect of viscosity is more significant in the downstream sections of the tube and as a result, the flow turning speed is increased, leading to a sharper streamline curvature near the wall. As concluded in Section 4.3.1, a more gradual flow turning occurs in case of expanding wall combined with injection, see Fig. 10a and in case of contracting wall combined with suction, see Fig. 10b.

Table 8
Radial velocity overshoots relative to the wall for different Re (analytical solution)

	$\alpha = 20$		$\alpha = -10$	
	r	v	r	v
$Re = 1000$	0.86023	−1.068464	0.86023	−1.065984
$Re = 100$	0.82462	−1.084838	0.87178	−1.058715
$Re = -50$	0.90554	−1.044215	0.83666	−1.086915
$Re = -100$	0.88318	−1.053519	0.84853	−1.076252
$Re = -1000$	0.86023	−1.065272	0.86023	−1.067752

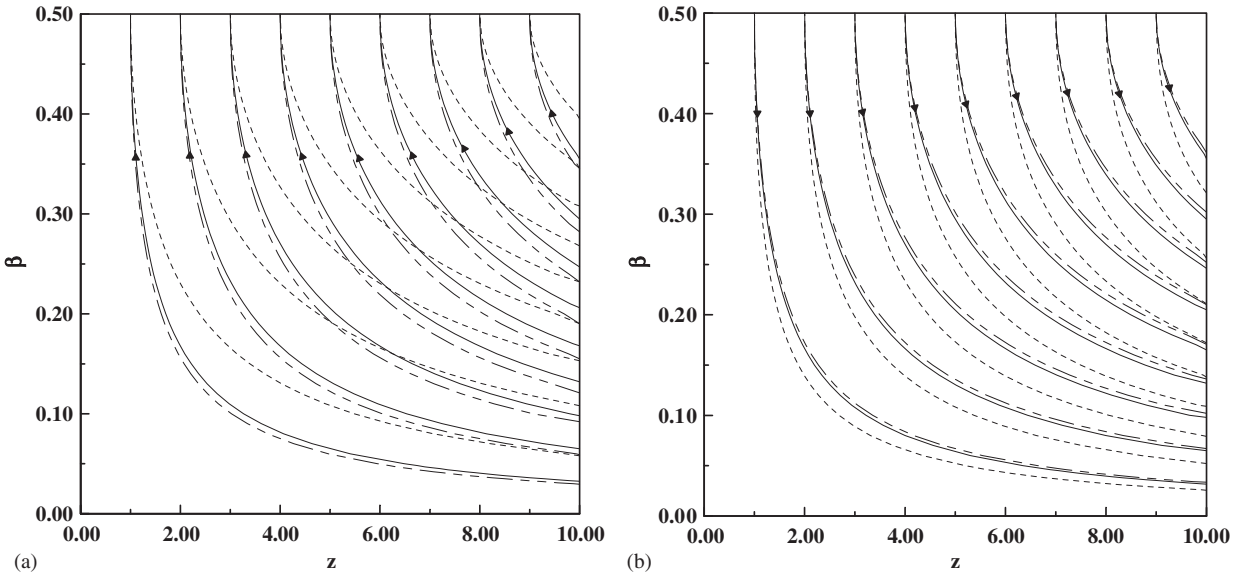

Fig. 9. Flow streamlines for $\alpha = 0$ ——, $\alpha = 50$ (· · · · · · · · ·) and $\alpha = -10$ (– · · – ··) at (a) $Re = -50$ and (b) $Re = 100$.

5. Vorticity, stress and pressure fields

5.1. Vorticity

For rotational flow, the curl of the velocity is non-zero which is the measure of vorticity. It is defined mathematically as

$$\bar{\omega} = |\nabla \times \bar{U}| = \frac{\partial \bar{v}}{\partial \bar{z}} - \frac{\partial \bar{u}}{\partial \bar{r}}. \tag{5.1}$$

Introducing dimensionless vorticity as $\omega = \bar{\omega} a / V$, Eq. (5.1) can be written as

$$\omega = \frac{\partial v}{\partial z} - \frac{\partial u}{\partial r}. \tag{5.2}$$

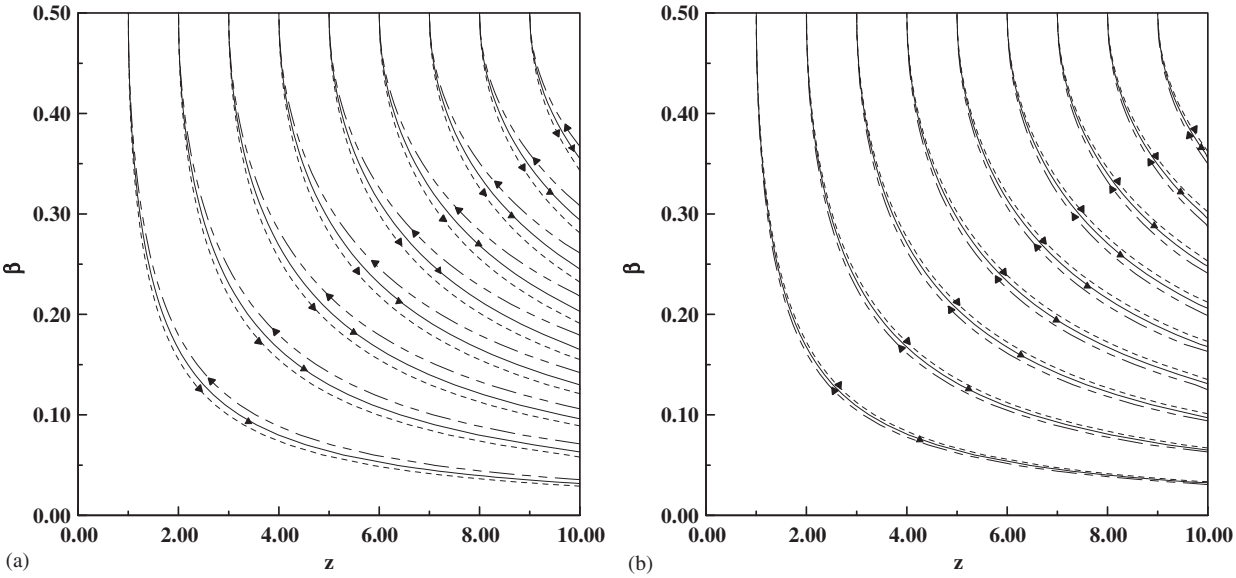

Fig. 10. Flow streamlines for $Re = 1000$ (—), $Re = 100$ $(\cdots\cdots)$ and $Re = -100$ $(- \cdot\cdot - \cdot\cdot)$ at (a) $\alpha = 20$ and (b) $\alpha = -10$.

Substituting (4.1) into (5.2) yields

$$\omega = -\frac{\partial u}{\partial r} = -z\sqrt{2\beta}\frac{\mathrm{d}^2 G}{\mathrm{d}\beta^2}. \tag{5.3}$$

5.2. Shear stress distribution

The shear stress can be determined from Newton's law for viscosity

$$\bar{\tau} = \mu\left[\frac{\partial \bar{v}}{\partial \bar{z}} + \frac{\partial \bar{u}}{\partial \bar{r}}\right] = -\mu\bar{\omega}. \tag{5.4}$$

Introducing the dimensionless shear stress $\tau = \bar{\tau}/(\rho V^2)$, Eq. (5.4) becomes

$$\tau = -K\omega. \tag{5.5}$$

We can get the stress at the wall by substituting in Eq. (5.3) $r = 1$, i.e., $\beta = \frac{1}{2}$, thus, Eq. (5.5) will take the form

$$\tau_{\mathrm{w}} = Kz\frac{\mathrm{d}^2 G(1/2)}{\mathrm{d}\beta^2}. \tag{5.6}$$

5.2.1. The effect of the wall expansion ratio α

Fig. 11 illustrates the behaviour of wall shear stress τ_w at different values of wall expansion ratio α, for fixed cross-flow Reynolds numbers $Re = 100$, 500 and 1000, respectively, along the wall surface. The shear stress along the wall surface increases in proportion to z. A first look shows that the greater sensitivity to wall expansion at $Re = 100$, see Fig. 11a. In case of expanding wall, the wall shear stress (absolute value) increases as α decreases, while it increases (absolute value) as $|\alpha|$ increases in case of contracting wall. That is because, as shown in Fig. 2, the greater the α is (case of expanding wall), the smaller the axial velocity near the wall surface, and the velocity gradient at the wall surface will be small, while the greater the $|\alpha|$ is (in case of contracting wall), the higher the axial velocity near the wall surface, and the velocity gradient at the wall surface will be high. The effect of suction on the wall shear stress for different values of wall expansion is illustrated in Fig. 12. The greater sensitivity to wall expansion appears at $Re = -50$, see Fig. 12a. The wall shear stress increases as α increases in case of expanding wall and it decreases as $|\alpha|$ increases in

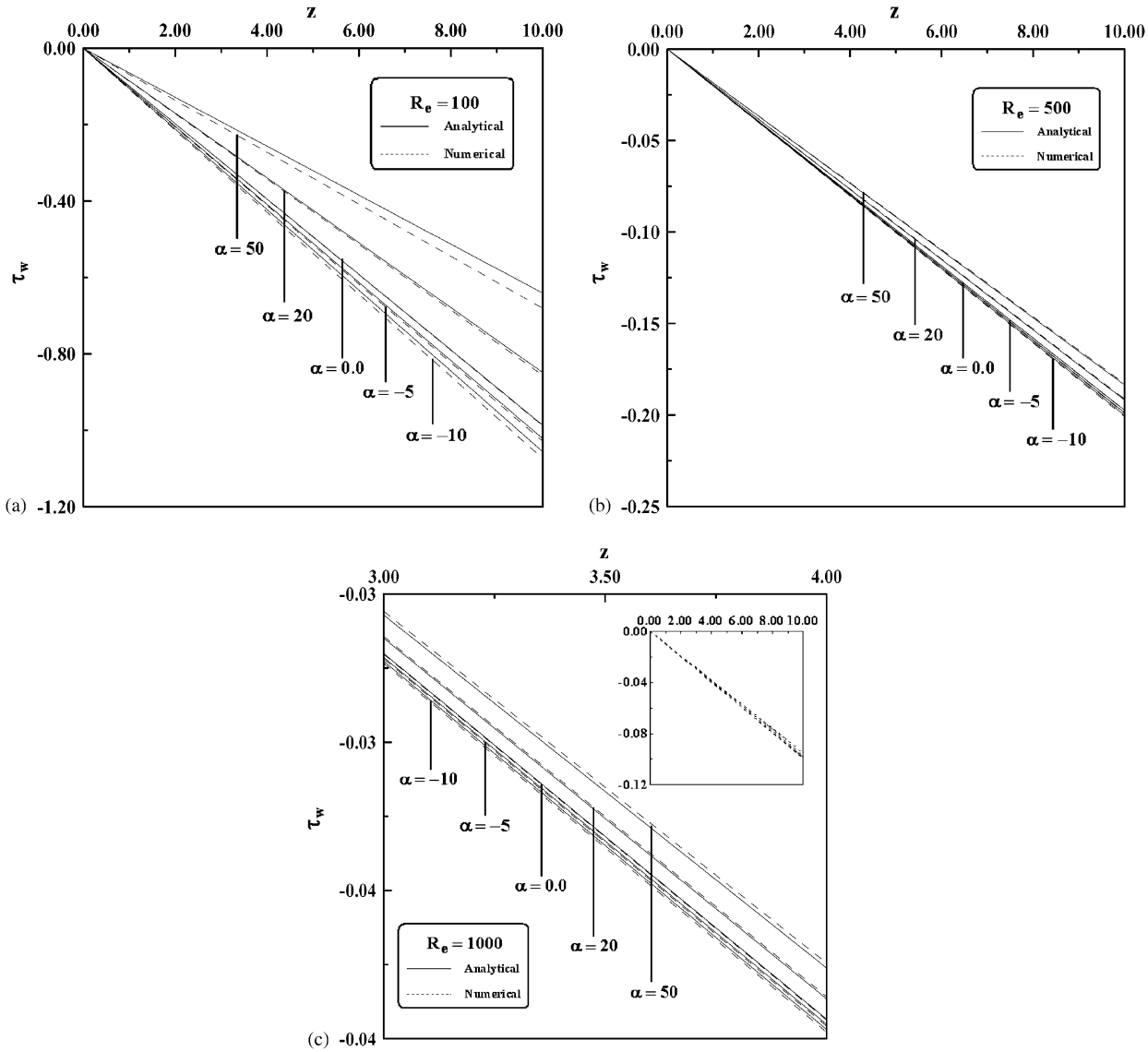

Fig. 11. Wall shear stress profiles shown over a range of α at (a) $Re = 100$, (b) $Re = 500$ and (c) $Re = 1000$.

case of contracting wall. This is as mentioned above. In cases, injection and suction, the wall shear stress decreases as $|Re|$ increases, see Figs. 11 and 12. This is due to the diminished role of viscosity at a higher Reynolds number. Comparing analytical and numerical solutions, the error in case of contracting wall combined with either suction or injection is very small compared with that of expanding wall combined with either suction or injection.

5.2.2. *The effect of cross-flow Reynolds number Re*

The effect of cross-flow Reynolds number Re on the wall shear stress τ_w, along the wall surface, for a fixed expansion ratios $\alpha = 20$ and -10, respectively, is illustrated in Fig. 13. In both cases, expanding and contracting walls, the wall shear stress (absolute value) decreases as Re increases (case of injection). Also it increases as $|Re|$ decreases (case of suction). This is due to the diminished role of viscosity at a higher Reynolds number. The analytical and numerical solutions become indistinguishable in both cases, expanding and contracting wall, combined with high $|Re|$. Also, a small error appears in both cases when combined with small $|Re|$, see Fig. 13.

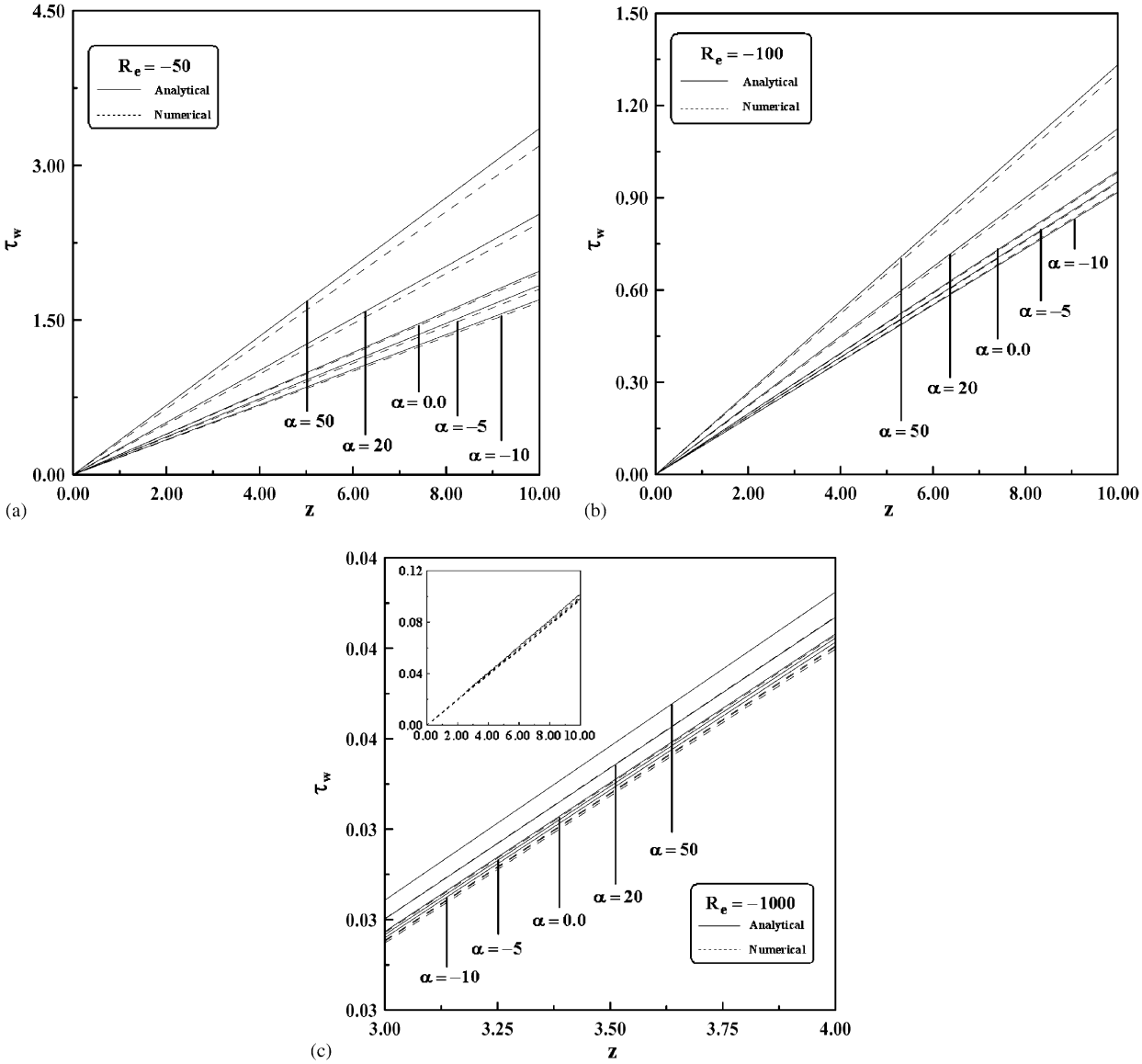

Fig. 12. Wall shear stress profiles shown over a range of α at (a) $Re = -50$, (b) $Re = -100$ and (c) $Re = -1000$.

5.3. Radial pressure distribution

To determine the radial pressure drop, substitute from (3.45) into (2.11) and use (3.49),

$$P_\beta = -\left[K G_\beta + K \alpha G + \frac{1}{\beta}\left(\frac{G}{2}\right)^2 \right]_\beta . \tag{5.7}$$

The radial pressure distribution can be determined by integrating (5.7) with the boundary conditions (3.51) and letting P_c be the centreline pressure, we get

$$\int_{P_c}^{P(\beta)} \mathrm{d}P = -\int_0^\beta \left[K G_\beta + K \alpha G + \frac{1}{\beta}\left(\frac{G}{2}\right)^2 \right] \mathrm{d}\beta. \tag{5.8}$$

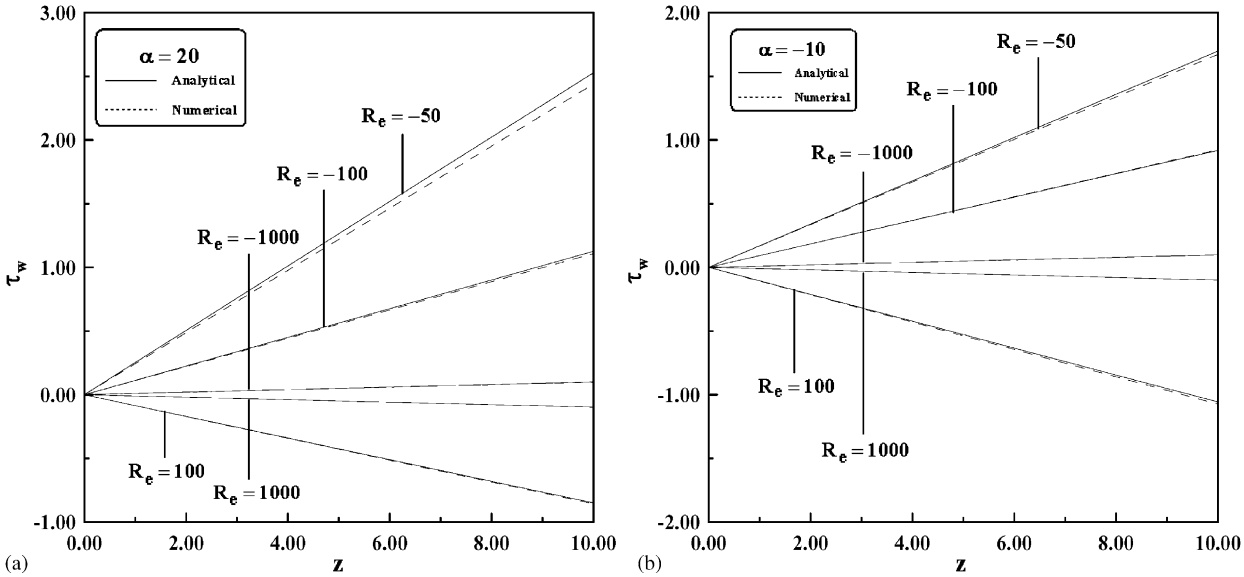

Fig. 13. Wall shear stress profiles shown over a range of Re at (a) $\alpha = 20$ and (b) $\alpha = -10$.

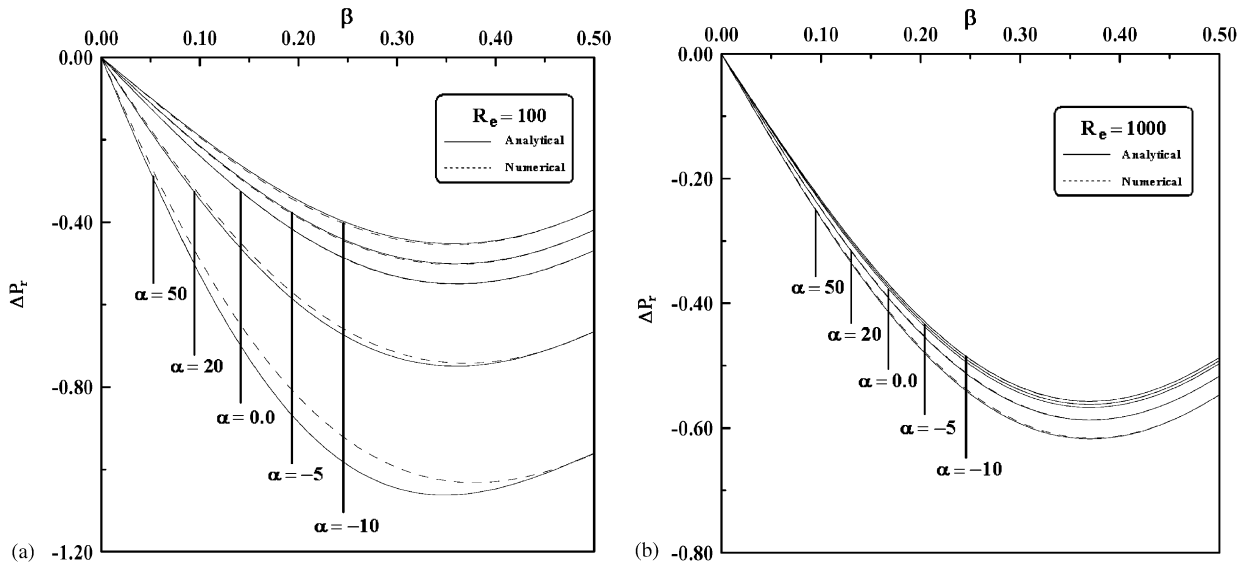

Fig. 14. Radial pressure distribution profiles shown over a range of α at (a) $Re = 100$ and (b) $Re = 1000$.

The resulting radial pressure drop will be

$$\Delta P_{\mathrm{r}} \equiv P(\beta) - P_{\mathrm{c}} = KG_{\beta}(0) - \left[KG_{\beta} + K\alpha G + \frac{1}{\beta}\left(\frac{G}{2}\right)^2 \right]. \tag{5.9}$$

5.3.1. The effect of the wall expansion ratio α

Fig. 14 illustrates the behaviour of the radial pressure drop ΔP_{r} at different values of wall expansion ratio α for fixed cross-flow Reynolds numbers $Re = 100$ and 1000, respectively. This behaviour is similar to the behaviour of the radial velocity (see Fig. 6). As seen, the whole central portion is higher than on the wall surface in pressure and the higher

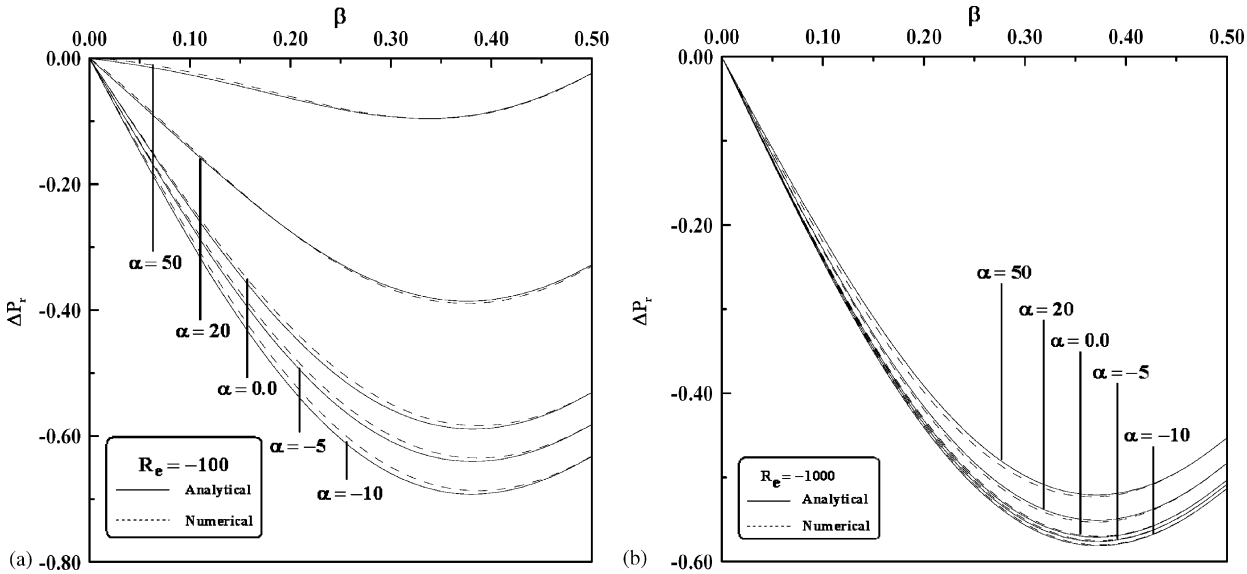

Fig. 15. Radial pressure distribution profiles shown over a range of α at (a) $Re = -100$ and (b) $Re = -1000$.

Table 9
Radial pressure drop overshoots relative to the wall in case of injection for different α (analytical solution)

	$Re = 100$		$Re = 1000$	
	r	ΔP_r	r	ΔP_r
$\alpha = 50$	0.83666	−1.062377	0.86023	−0.6175179
$\alpha = 20$	0.84853	−0.7486982	0.86023	−0.5872490
$\alpha = 0$	0.84853	−0.5496595	0.86023	−0.5671443
$\alpha = -5$	0.84853	−0.5006549	0.86023	−0.5621278
$\alpha = -10$	0.84853	−0.4521734	0.86023	−0.5571153

Table 10
Radial pressure drop overshoots relative to the wall in case of suction for different α (analytical solution)

	$Re = -100$		$Re = -1000$	
	r	ΔP_r	r	ΔP_r
$\alpha = 50$	0.82462	−0.0956602	0.86023	−0.5208311
$\alpha = 20$	0.87178	−0.3856838	0.86023	−0.5509211
$\alpha = 0$	0.87178	−0.5888647	0.86023	−0.5710558
$\alpha = -5$	0.87178	−0.6404785	0.86023	−0.5760981
$\alpha = -10$	0.87178	−0.6924208	0.86023	−0.5811445

the expansion ratio is (case of expanding wall), the higher the radial pressure drop (absolute value). Also, the higher the $|\alpha|$ (case of contracting wall), the lower the radial pressure drop (absolute value). The effect of suction on the radial pressure drop at different values of α is illustrated in Fig. 15. The higher the expansion ratio is (case of expanding wall), the lower the radial pressure drop (absolute value). Also, the higher the $|\alpha|$ (case of contracting wall), the higher the radial pressure drop (absolute value). As concluded in Section 4.2.1, there exists a point along the interval $0 < \beta < 0.5$, such that the radial pressure drop overshoots relative to its value at the wall. Tables 9 and 10 indicate these points and the corresponding radial pressure drop overshoots relative to the wall.

Table 11
Comparison between analytical and numerical solutions for radial pressure drop at $\beta = 0.15$

ΔP_r at	$Re = 100$		Percentage error (%)	$Re = -100$		Percentage error (%)
$\beta = 0.15$	Analytical	Numerical		Analytical	Numerical	
$\alpha = 50$	−0.73192	−0.70886	3.15062	−0.04437	−0.04298	3.13275
$\alpha = 20$	−0.48601	−0.47238	2.80447	−0.21266	−0.21042	1.05332
$\alpha = 0.0$	−0.34175	−0.34217	0.12290	−0.34453	−0.33707	2.16527
$\alpha = -5$	−0.30814	−0.31079	0.86000	−0.37996	−0.37211	2.06601
$\alpha = -10$	−0.27552	−0.27994	1.60424	−0.41638	−0.40575	2.55296

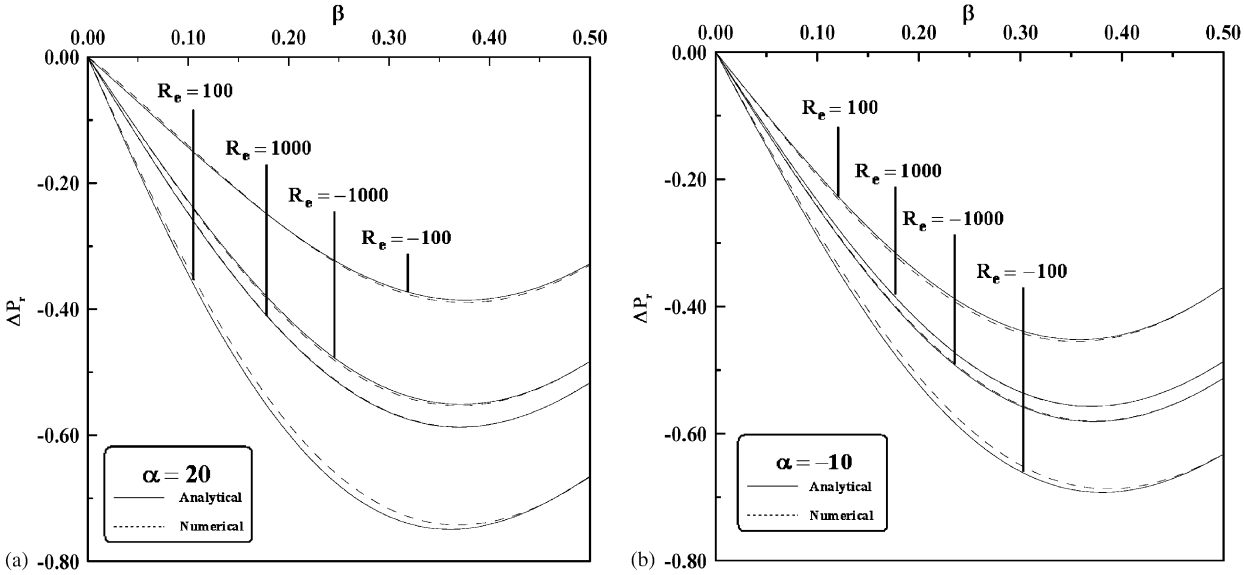

Fig. 16. Radial pressure distribution profiles shown over a range of Re at (a) $\alpha = 20$ and (b) $\alpha = -10$.

In case of injection, the smallest overshoots (absolute value) with the closest distance to the wall appear when wall expansion ratio is small enough (in case of expanding wall) or high enough (in case of contracting wall), see Table 9, while in case of suction, the smallest overshoots (absolute value) with the closest distance to the wall appear when wall expansion ratio is high enough (in case of expanding wall) or low enough (in case of contracting wall), see Table 10. Table 11 illustrates the comparison between the analytical and numerical solutions of the radial pressure drop at different values of wall expansion ratio for cross-flow Reynolds number $Re = 100$ and -100. In both cases, injection with $Re = 100$ and suction with $Re = -100$, the percentage error increases as $|\alpha|$ increases, especially, in case of expanding wall with $\alpha = 50$, see Table 11.

5.3.2. *The effect of the cross-flow Reynolds number Re*

The effect of the cross-flow Reynolds number Re on the radial pressure drop ΔP_r for fixed wall expansion ratios is illustrated in Fig. 16. By comparison to Figs. 14 and 15, similar conclusions can be deduced. In case of expanding wall combined with injection, the radial pressure drop decreases (absolute value) with increasing Re and it increases (absolute value) with increasing $|Re|$ in case of expanding wall combined with suction, see Fig. 16a. In case of contracting wall combined with injection, the radial pressure drop increases (absolute value) with increasing Re and it decreases (absolute value) with increasing $|Re|$ in case of contracting wall combined with suction, see Fig. 16b.

The analytical and numerical solutions become indistinguishable in cases, expanding and contracting wall, combined with high $|Re|$. A small error appears in both cases when combined with small $|Re|$, see Fig. 16.

Table 12
Radial pressure overshoots relative to the wall for different Re (analytical solution)

	$\alpha = 20$		$\alpha = -10$	
	r	ΔP_r	r	ΔP_r
$Re = 1000$	0.86023	−0.5872490	0.86023	−0.5571153
$Re = 100$	0.84853	−0.7486982	0.84853	−0.4521734
$Re = -100$	0.87178	−0.3856838	0.87178	−0.6924208
$Re = -1000$	0.86023	−0.5509211	0.86023	−0.5811445

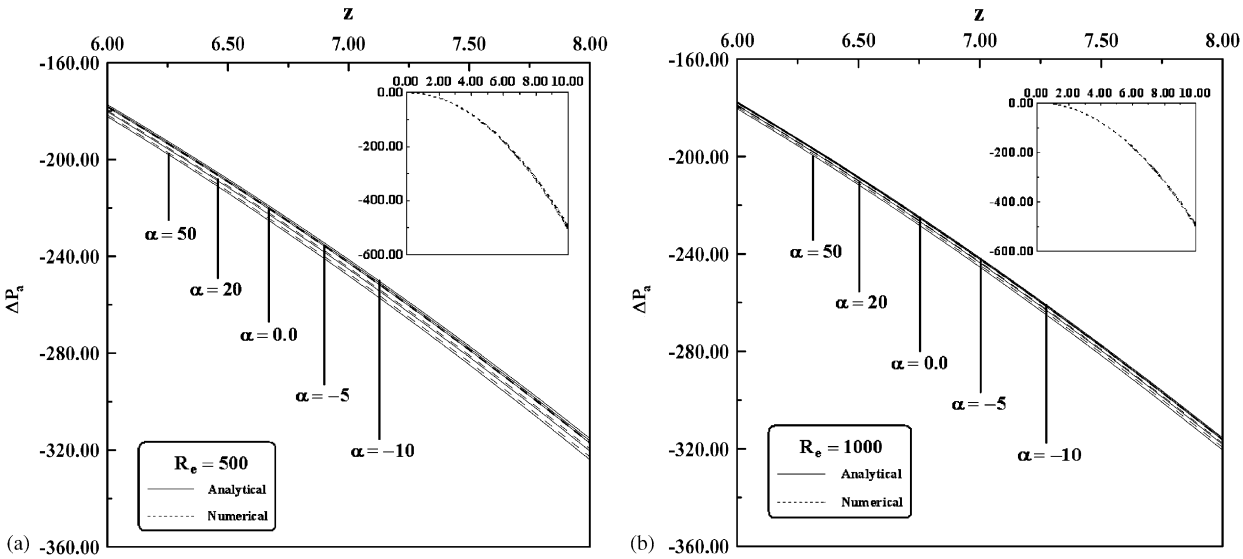

Fig. 17. Axial pressure distribution profiles shown over a range of α at (a) $Re = 500$ and (b) $Re = 1000$.

The points that lie in the interval $0 < \beta < 0.5$, such that the radial pressure drop exceeds its value at the wall, are indicated in Table 12.

5.4. Axial pressure distribution

Substituting (3.45) into (2.10) and using (3.49), we get

$$P_z = z\left[K\left(2\beta\frac{\mathrm{d}^3G}{\mathrm{d}\beta^3} + (2\alpha\beta+2)\frac{\mathrm{d}^2G}{\mathrm{d}\beta^2} + 2\alpha\frac{\mathrm{d}G}{\mathrm{d}\beta}\right) + G\,\frac{\mathrm{d}^2G}{\mathrm{d}\beta^2} - \left(\frac{\mathrm{d}G}{\mathrm{d}\beta}\right)^2\right]. \tag{5.10}$$

The resulting axial pressure will be

$$\Delta P_\mathrm{a} = \frac{1}{2}\,z^2\left[K\left(2\beta\frac{\mathrm{d}^3G}{\mathrm{d}\beta^3} + (2\alpha\beta+2)\frac{\mathrm{d}^2G}{\mathrm{d}\beta^2} + 2\alpha\,\frac{\mathrm{d}G}{\mathrm{d}\beta}\right) + G\frac{\mathrm{d}^2G}{\mathrm{d}\beta^2} - \left(\frac{\mathrm{d}G}{\mathrm{d}\beta}\right)^2\right]. \tag{5.11}$$

5.4.1. The effect of the wall expansion ratio α

Fig. 17 illustrates the behaviour of axial pressure drop ΔP_a at different values of wall expansion ratio α for fixed cross-flow Reynolds numbers $Re = 500$ and 1000, respectively. It takes a parabolic form along the axis of the pipe. The axial pressure drop increases (absolute value) as α increases in case of expanding wall and it decreases as $|\alpha|$ increases in case of contracting wall. The effect of suction on the axial pressure distribution at different values of wall

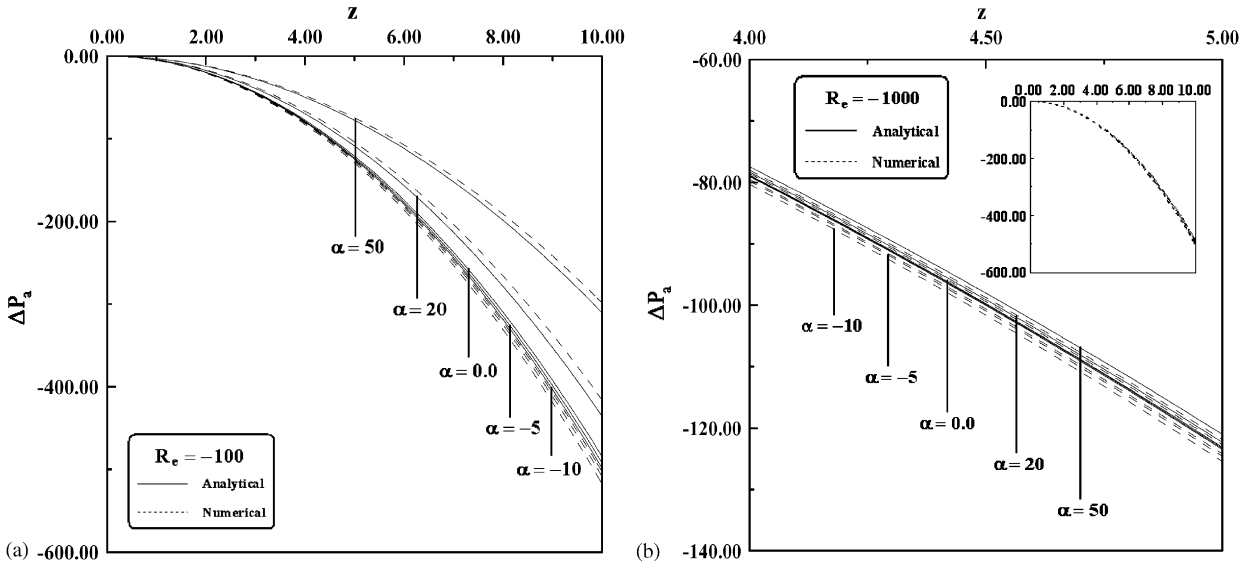

Fig. 18. Axial pressure distribution profiles shown over a range of α at (a) $Re = -100$ and (b) $Re = -1000$.

expansion ratio is shown in Fig. 18. The greater sensitivity to wall expansion appears at $Re = -100$, see Fig. 18a. The axial pressure drop ΔP_a increases as α decreases in case of expanding wall and it increases as $|\alpha|$ increases in case of contracting wall. Comparing analytical and numerical solutions as seen in magnified portions of Fig. 17, one notes that, a small error appears in case of expanding wall combined with injection with $Re = 500$, see Fig. 17a. The analytical and numerical solutions become indistinguishable in case of injection with $Re = 1000$, combined with both expanding and contracting wall, see Fig. 17b. A small error appears in case of suction with $Re = -100$ combined with expanding wall, see Fig. 18a.

5.4.2. The effect of the cross-flow Reynolds number Re

The effect of the cross-flow Reynolds number Re on the axial pressure drop ΔP_a for fixed wall expansion ratios is illustrated in Fig. 19. By comparison to Figs. 17 and 18, similar conclusions can be deduced. In case of expanding wall combined with injection, the axial pressure drop increases (absolute value) with decreasing Re and it increases (absolute value) with increasing $|Re|$ in case of expanding wall combined with suction, see Fig. 19a. In case of contracting wall combined with injection, the axial pressure drop increases (absolute value) with increasing Re and it increases (absolute value) with decreasing $|Re|$ in case of contracting wall combined with suction, see Fig. 19b. Comparing analytical and numerical solutions as seen in magnified portions of Fig. 19, one notes that a small error appears in case of contracting wall combined with suction, see Fig. 19b. Also a small error appears in case of expanding wall combined with suction, see Fig. 19a.

6. Conclusions

Lie-group method is applicable to both linear and non-linear partial differential equations, which leads to similarity variables that may be used to reduce the number of independent variables in partial differential equations. By determining the transformation group under which a given partial differential equation is invariant, we can obtain information about the invariants and symmetries of that equation. This information can be used to determine the similarity variables that will reduce the number of independent variables in the system. In this work, we have used Lie symmetry techniques to obtain similarity reductions of nonlinear equations of motion (2.1)–(2.3) which describe the unsteady incompressible laminar flow in a semi-infinite porous circular pipe with injection or suction through the pipe wall. This analysis simulates the flow field by the burning of inner surface of cylindrical grain in a circular-port rocket motor.

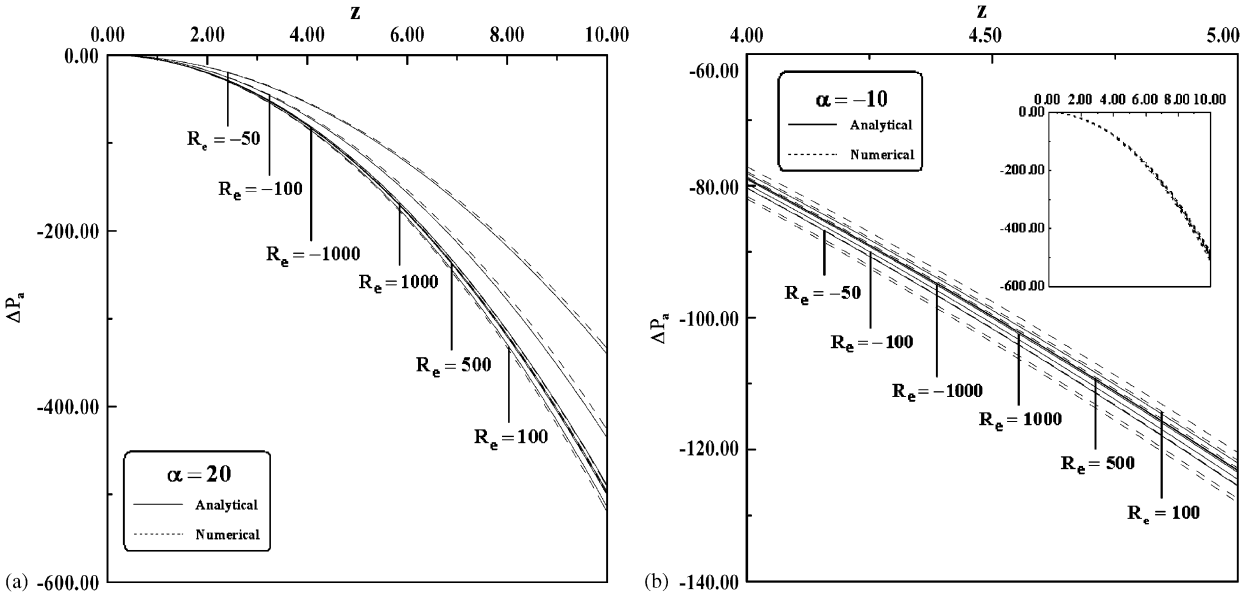

Fig. 19. Axial pressure distribution profiles shown over a range of Re at (a) $\alpha = 20$ and (b) $\alpha = -10$.

By determining the transformation group under which a given partial differential equation is invariant, we obtained information about the invariants and symmetries of that equation. This information, in turn, was used to determine similarity variables that reduced the number of independent variables. With constant wall expansion ratio, we get a fourth-order ordinary differential equation (3.50) with boundary condition (3.51), which has been solved using small-parameter perturbations and the results are compared with numerical solutions using shooting method coupled with Runge–Kutta scheme. We have studied and plotted the effects of cross-flow Reynolds number and wall expansion ratio on velocity, flow streamlines, axial and radial pressure, and wall shear stress. We found that the numerical solution is in a good agreement with the analytical solution.

Acknowledgement

The authors would like to thank the referee for suggesting certain changes in the original manuscript, for his valuable comments which improved the paper and for his great interest in that work.

References

[1] P. Basarab, V. Lahno, Group classification of nonlinear partial differential equations: a new approach to resolving the problem, in: Proceedings of Institute of Mathematics of NAS of Ukraine, vol. 43, 2002, pp. 86–92.

[2] G.I. Burde, Expanded Lie group transformations and similarity reductions of differential equations, in: Proceedings of Institute of Mathematics of NAS of Ukraine, vol. 43, 2002, pp. 93–101.

[3] M.L. Gandarias, M.S. Bruzon, Classical and nonclassical symmetries of a generalized Boussinesq equation, J. Nonlinear Math. Phys. 5 (1998) 8–12.

[4] M. Goto, S. Uchida, Unsteady flows in a semi-infinite expanding pipe with injection through wall, Trans. Japan Soc. Aeronautical and Space Sci. 33 (9) (1990) 14–27.

[5] J.M. Hill, Solution of Differential Equations by Means of One-Parameter Groups, Pitman Publishing Co., 1982.

[6] P.E. Hydon, Symmetry Methods for Differential Equations, Cambridge University Press, Cambridge, MA, 2000.

[7] N.H. Ibragimov, Elementary Lie Group Analysis and Ordinary Differential Equations, Wiley, New York, 1999.

[8] J. Magdalani, A.B. Vyas, G.A. Flandro, Higher mean-flow approximation for solid rocket motors with radially regressing walls, AIAA J. 40 (9) (2002) 1780–1788.

[9] B. Moritz, W. Schwalm, D. Uherka, Finding Lie groups that reduce the order of discrete dynamical systems, J. Phys. A 31 (1998) 7379–7402.

[10] M.C. Nucci, P.A. Clarkson, The nonclassical method is more general than the direct method for symmetry reductions. An example of the Fitzhugh–Nagumo equation, Phys. Lett. A 164 (1992) 49–56.
[11] P.J. Olver, Applications of Lie Groups to Differential Equations, Springer, New York, 1986.
[12] I. Proudman, K. Johnson, Boundary layer growth near a rear stagnation point, J. Fluid Mech. 12 (1962) 161–168.
[13] R. Seshadri, T.Y. Na, Group Invariance in Engineering Boundary Value Problems, Springer, New York, 1985.
[14] R.M. Terrill, On some exponentially small terms arising in flow through a porous pipe, Quart. J. Mech. Appl. Math. 26 (3) (1973) 347–354.
[15] R.M. Terrill, P.W. Thomas, On laminar flow through a uniformly porous pipe, Appl. Sci. Res. 21 (1969) 37–67.
[16] Z. Yi, M. Fengxiang, Lie symmetries of mechanical systems with unilateral holonomic constraints, Chinese Sci. Bull. 45 (2000) 1354–1358.